



## Adding a new dimension: Multi-level structure and organization of mixed-species *Pseudomonas aeruginosa* and *Staphylococcus aureus* biofilms in a 4-D wound microenvironment

Radhika Dhekane<sup>a</sup>, Shreeya Mhade<sup>b</sup>, Karishma S. Kaushik<sup>a,\*</sup>

<sup>a</sup> Department of Biotechnology, Savitribai Phule Pune University, Pune, India

<sup>b</sup> Department of Bioinformatics, Guru Nanak Khalsa College of Arts, Science and Commerce (Autonomous), Mumbai, India

### ARTICLE INFO

#### Keywords:

Biofilms  
Microenvironment  
Wounds  
Structure  
Organization  
Mixed-species  
*Pseudomonas aeruginosa*  
*Staphylococcus aureus*  
In vitro wound milieu (IVWM)  
BiofilmQ

### ABSTRACT

Biofilms in wounds typically consist of aggregates of bacteria, most often *Pseudomonas aeruginosa* and *Staphylococcus aureus*, in close association with each other and the host microenvironment. Given this, the interplay across host and microbial elements, including the biochemical and nutrient profile of the microenvironment, likely influences the structure and organization of wound biofilms. While clinical studies, *in vivo* and *ex vivo* model systems have provided insights into the distribution of *P. aeruginosa* and *S. aureus* in wounds, they are limited in their ability to provide a detailed characterization of biofilm structure and organization across the host-microbial interface. On the other hand, biomimetic *in vitro* systems, such as host cell surfaces and simulant media conditions, albeit reductionist, have been shown to support the co-existence of *P. aeruginosa* and *S. aureus* biofilms, with species-dependent localization patterns and interspecies interactions. Therefore, composite *in vitro* models that bring together key features of the wound microenvironment could provide unprecedented insights into the structure and organization of mixed-species biofilms. We have built a four-dimensional (4-D) wound microenvironment consisting of a 3-D host cell scaffold of co-cultured human epidermal keratinocytes and dermal fibroblasts, and an *in vitro* wound milieu (IVWM); the IVWM provides the fourth dimension that represents the biochemical and nutrient profile of the wound infection state. We leveraged this 4-D wound microenvironment, in comparison with biofilms in IVWM alone and standard laboratory media, to probe the structure of mixed-species *P. aeruginosa* and *S. aureus* biofilms across multiple levels of organization such as aggregate dimensions and biomass thickness, species co-localization and spatial organization within the biomass, overall biomass composition and interspecies interactions. In doing so, the 4-D wound microenvironment platform provides multi-level insights into the structure of mixed-species biofilms, which we incorporate into the current understanding of *P. aeruginosa* and *S. aureus* organization in the wound bed.

### 1. Introduction

Biofilms are multicellular microbial communities, implicated in chronic wound infections, where they fuel persistent, non-healing wounds [1–4]. In chronic wounds, biofilms are seen as discrete, microbial aggregates distributed across, and in close association with, wound bed [5–11]. Under these conditions, biofilm aggregates interface with a range of microenvironmental factors including host cells, such as dermal fibroblasts and epidermal keratinocytes, as well as matrix, biochemical and nutrient factors [12–15]. Further, biofilms in wounds often consist of more than one microbial species [3,9,10,16,17]; *Pseudomonas aeruginosa* and *Staphylococcus aureus* are the most common

bacterial co-pathogens [18–22]. Consequently, *P. aeruginosa* and *S. aureus* have been observed to co-exist in the wound bed, with distinct structural and organizational features. In biopsies of chronic wounds, *P. aeruginosa* and *S. aureus* aggregates exist in distinct regions, albeit separated by a few hundred micrometers [6]. On the other hand, in *in vivo* wound models, the two species exist in close proximity, with bacterial clusters observed to overlap with each other [18,20]. While the presence of truly-mixed aggregates with both species might be debated, *P. aeruginosa* and *S. aureus* have been detected in chronic wound biofilm aggregates consisting of bacteria of different species and morphologies, including bacilli and cocci [1,9–11]. Given this, it is very likely that during initial infection, or at some point in the progression of the

\* Corresponding author.

E-mail address: [karishmaskaushik@unipune.ac.in](mailto:karishmaskaushik@unipune.ac.in) (K.S. Kaushik).

<https://doi.org/10.1016/j.biofilm.2022.100087>

Received 15 May 2022; Received in revised form 20 September 2022; Accepted 11 October 2022

Available online 20 October 2022

2590-2075/© 2022 The Authors. Published by Elsevier B.V. This is an open access article under the CC BY-NC-ND license (<http://creativecommons.org/licenses/by-nc-nd/4.0/>).

infected wound state, *P. aeruginosa* and *S. aureus* exist in close proximity with each other, allowing for possible interspecies interactions [19,23]. Therefore, in the complex wound microenvironment, the interplay across host and microbial elements likely influences the structure and organization of mixed-species bacterial biofilms.

The vast majority of laboratory studies on wound biofilms employ two-dimensional (2-D) plastic surfaces and refined protein broths [24–28], in which biofilms are grown as homogeneous dense mats or mushroom-like microcolonies [29–31]. This is clearly different from conditions and observations in clinical wounds, and are therefore of limited relevance. While *in vivo* and *ex vivo* systems have provided more relevant insights into the dimensions and distribution of biofilm aggregates [6–8,32–34], they present technical and scientific challenges with respect to a detailed analysis of biofilm structure across the host-microbial interface. More recently, there has been a push towards developing engineered *in vitro* approaches that recapitulate key features of the wound infection state, and enable the study of wound biofilms in the context of the complex microenvironment [13,18,35,36]. These approaches include reconstructed *in vitro* systems, such as mixed-species biofilms on 3-D host cell surfaces, and in simulant media conditions that mimic the wound milieu [13,18,35,37–39]. In these recapitulated systems, biofilm aggregates display species-dependent localization patterns and characteristic interspecies interactions [13,18,35], underscoring their role as relevant and tractable platforms.

To study the structure and organization of mixed-species biofilms under conditions that mimic the infection state, we have built a four-dimensional (4-D) wound microenvironment consisting of a 3-D reconstructed host cell surface and an *in vitro* wound milieu (IVWM). The 3-D host cell scaffold consists of human epidermal keratinocytes (HaCaT) and human dermal fibroblasts (HDFa), which are co-cultured and fixed to serve as a biomimetic substratum. In our previous work, we developed and evaluated an IVWM that recapitulates the composition of clinical wound fluid, consisting of serum along with matrix elements such as collagen, fibrinogen, and fibronectin, and biochemical factors such as lactic acid and lactoferrin [35]. In doing so, the IVWM provides the fourth dimension that represents the biochemical and nutrient profile of the wound infection state. Using confocal fluorescence microscopy and quantitative image analysis, we leveraged this recapitulated 4-D microenvironment to characterize structure of mixed-species *P. aeruginosa* and *S. aureus* biofilms across multiple levels of organization, such as aggregate dimensions and biomass thickness, species co-localization and spatial organization within the biomass, overall biomass composition and interspecies interactions. To understand the possible roles of the host cell scaffold and IVWM, and to compare with laboratory media conditions, mixed-species biofilms grown in IVWM and Luria-Bertani (LB) media were also analyzed. Further, to understand the role of interspecies interactions, *P. aeruginosa* and *S. aureus* were grown as single-species biofilms in the different conditions. Taken together, our findings provide multi-level insights into mixed-species *P. aeruginosa* and *S. aureus* biofilms under wound-relevant conditions, which we incorporate into the current understanding of *P. aeruginosa* and *S. aureus* organization in the wound bed.

## 2. Materials and methods

### 2.1. Bacterial strains and growth conditions

*Pseudomonas aeruginosa* (PAO1-pUCP18::mCherry, Amp/Carb<sup>R</sup>) and *Staphylococcus aureus* (Strain AH13-pAH13::GFP<sub>uvr</sub>, Erm<sup>R</sup>) were gifted by Dr. Derek Fleming and Dr. Kendra Rumbaugh (Texas Tech University Health Science Center, Lubbock, Texas, USA) [40,41]. For all experiments, *P. aeruginosa* was grown in LB medium (broth: Sigma, USA, L3022; agar: SRL, India, 474236) containing 100 µg/mL ampicillin (HiMedia, India, TC021), and *S. aureus* was grown in LB medium containing 10 µg/mL erythromycin (Himedia, India, TC024). *P. aeruginosa* and *S. aureus* were streaked on antibiotic-containing LB agar and

incubated at 37 °C. For overnight cultures, isolated colonies from streaked agar plates were grown in antibiotic-containing LB broth at 37 °C under shaking conditions for 18–20 h.

### 2.2. Minimum inhibitory concentration (MIC) by broth dilution method

The broth microdilution assay was performed to determine the MIC of ampicillin for *S. aureus* (Strain AH13-pAH13::GFP<sub>uvr</sub>, Erm<sup>R</sup>) using the method described previously [42,43]. Briefly, an overnight culture of *S. aureus* was washed once in LB medium, and diluted to a density of  $2 \times 10^7$  cells/mL in fresh LB. From this dilution, 50 µL of bacterial suspension and 50 µL of ampicillin (in dilutions from 0.03125 µg/mL to 512 µg/mL, prepared in LB medium) were dispensed in each well of a 96-well plate (Corning, USA, 3603; three replicates). A sterility control consisting of 100 µL of only LB medium (without bacteria) was also set up (in triplicate). The 96-well plate was incubated at 37 °C under shaking conditions for ~18–20 h. Following this, optical density was measured at 600 nm, and percent inhibition was calculated as follows:  $(OD_{600}$  at 0 µg/mL -  $OD_{600}$  at a given concentration) /  $OD_{600}$  at 0 µg/mL) × 100. The lowest concentration of ampicillin that showed 90% inhibition was considered as the MIC. Using this method, the MIC<sub>90</sub> of ampicillin for *S. aureus* was determined to be 0.25 µg/mL.

### 2.3. Host cell culture and maintenance

Primary human dermal fibroblasts (HDFa) were purchased from PromoCell (Germany, C-12302) and cultured in Fibroblast Growth Medium (FGM) [Cell Applications, USA 116–500; medium contains 2% fetal bovine serum (FBS)]. The immortalized epidermal keratinocyte cell line (HaCaT) was a gift from Dr. Madhur Motwani (Linq Labs, Pune, India) and was cultured in Keratinocyte serum-free Growth Medium (KGM) (Cell Applications, USA, 131–500A) supplemented with 1% FBS (Gibco, Brazil, 10270106). The cells were grown in tissue-culture treated, 25 cm<sup>2</sup> culture flasks (Tarsons, Korea, 950040) and maintained at 37 °C in a 5% CO<sub>2</sub> humidified incubator. For all experiments, HDFa cells had passage numbers <10 and HaCaT cells had passage numbers between 10 and 20.

### 2.4. Preparation of the *in vitro* wound milieu (IVWM)

The *in vitro* wound milieu (IVWM) was prepared with FBS as the base component, with the addition of collagen, fibronectin, fibrinogen, lactic acid, and lactoferrin, as previously described [35]. Fibrinogen (Sigma, USA, F3879) was dissolved in filter-sterilized (0.2 µm pore size, Cole-Parmer, India, WW-15945-52), pre-warmed saline (0.9% NaCl, Merck, India, 106404) to the concentration of 10 mg/mL and stored at –20 °C. Fibronectin (Sigma, USA, F4759) was dissolved in autoclaved distilled water to the concentration of 1 mg/mL and stored at –20 °C. Peptone water (0.1% w/v) was prepared by dissolving peptone (SRL, India, 95292) in 0.9% NaCl, and autoclaved and stored at 4 °C. Lactoferrin (2 mg/mL) (Sigma, USA, L4040) was prepared in PBS (pH 7.2, Thermo Fisher Scientific, USA, 20012027), filter-sterilized and stored at 4 °C. Commercial FBS (Gibco, Brazil, 10270106) was stored at 4 °C. Rat tail collagen (50 µg/mL in 0.02 M acetic acid) (Sigma, USA, 12220) was stored at 4 °C. Lactic acid (≥85%; Sigma, USA, W261114) was stored at room temperature. Components stored at –20 °C were thawed on ice prior to reconstitution of the IVWM. The IVWM was prepared by adding the above components to FBS (final concentration in IVWM, 70%) as follows (numbers indicate final concentrations): fibrinogen (300 µg/mL), fibronectin (30 µg/mL), rat-tail collagen (12 µg/mL), lactoferrin (20 µg/mL) and lactic acid (11 mM). Reconstituted IVWM was freshly prepared prior to all experiments.

### 2.5. Preparation of host cell scaffolds

HaCaT and HDFa cells were grown in cell culture flasks up to

80–90% confluency. Cells were trypsinized with 700  $\mu$  L of 0.25% Trypsin-EDTA solution (Gibco, Canada, 25200056), followed by the addition of 700  $\mu$  L KGM with 1% FBS (for HaCaT) or FGM (for HDFa). To prepare co-cultured scaffolds of HDFa and HaCaT cells, 50  $\mu$  L of  $1 \times 10^5$  cells/mL (~5000 cells of HaCaT cells in serum-free KGM) and 50  $\mu$  L of  $1 \times 10^5$  cells/mL of HDFa cells (~5000 cells in FGM containing 2% FBS) were added to a single well of 96 - well flat, clear bottom, tissue culture treated, black polystyrene microplate (Corning, USA, 3603), and grown in a 5% CO<sub>2</sub> humidified incubator at 37 °C for 72 h [44]. Following this, the supernatant medium was removed, and the confluent cells were fixed in 50  $\mu$  L of 4% paraformaldehyde (PFA) (Sigma, USA, 158127) for 10 min at room temperature. Fixed cells were rinsed in 200  $\mu$  L sterile PBS four times, and stored in 200  $\mu$  L sterile PBS at 4 °C until further use. Prior to experiments, fixed cell scaffolds were stained with 50  $\mu$  L of filter-sterilized 30  $\mu$  M 4',6-Diamidino-2-Phenylindole, Dihydrochloride (DAPI) (Invitrogen, Germany, D1306) for 5 min at room temperature, followed by two rinses with 200  $\mu$  L PBS each.

## 2.6. Growth of mixed-species and single-species biofilms in the 4-D wound microenvironment, IVWM only and LB media

Overnight cultures of *P. aeruginosa* and *S. aureus* (set up in antibiotic-containing LB medium, 100  $\mu$  g/mL ampicillin for *P. aeruginosa* and 10  $\mu$  g/mL erythromycin for *S. aureus*) were centrifuged at 4000 rpm for 5 min at 25 °C, following which the supernatant was removed and the pellet was resuspended in 1 mL LB medium without antibiotics. Optical density of this suspension was measured at 600 nm, and the bacterial density was adjusted in LB medium without antibiotics. From this suspension, bacterial cultures were each diluted to  $2 \times 10^7$  cells/mL in freshly-prepared IVWM or LB medium (antibiotic-free). For mixed-species biofilms, 50  $\mu$  L of *P. aeruginosa* and 50  $\mu$  L of *S. aureus* diluted in IVWM (~ $10^6$  cells each) were added to fixed HDFa + HaCaT host cell scaffolds. For single-species biofilms, 50  $\mu$  L of *P. aeruginosa* or *S. aureus* diluted in IVWM (~ $10^6$  cells) were added to fixed HaCaT + HDFa host cell scaffolds, followed by the addition of 50  $\mu$  L of IVWM to make a total volume of 100  $\mu$  L. The 4D microenvironment, including microbial cells, host cell scaffolds and the IVWM, was incubated at 37 °C in a static incubator for 4, 8, 24 and 48 h. Given the possible detrimental effects of laser exposure on bacterial growth, biofilm wells for different time points were seeded together and images for each time point were obtained from a different well. As controls, host cell scaffolds were also incubated with IVWM only (without bacteria). In the case of IVWM alone and LB media, mixed-species or single-species biofilms were set up as above (in IVWM or LB media), and inoculated into wells without host cell scaffolds. Based on the protocol above, the initial inoculum for the mixed-species biomass is double that in the single-species biomass. This allows the direct comparison of *P. aeruginosa* and *S. aureus* biofilms under mixed-species and single-species biofilms over time, with the same initial bacterial count for a given species across the conditions. While this two-fold difference in total inoculum density could alter nutrient availability in mixed-species and single-species conditions, both IVWM and LB medium are highly nutrient-rich in composition. It is also important to clarify that since the bacterial suspensions were grown overnight in antibiotic-containing LB media (100  $\mu$  g/mL ampicillin for *P. aeruginosa* and 10  $\mu$  g/mL erythromycin for *S. aureus*) and inoculated in IVWM, the resultant IVWM would contain a small proportion of LB media (estimated as less than 2% of the final composition of IVWM). While *P. aeruginosa* is inherently resistant to erythromycin, the residual concentration of ampicillin could influence growth of *S. aureus*. However, overnight bacterial suspensions in antibiotic-containing LB media were pelleted and resuspended in antibiotic-free LB media, followed by further dilution in antibiotic-free LB media, and inoculation into IVWM to obtain the desired bacterial densities. Based on the volumes of media used for the dilutions, any residual ampicillin from the pellet or resuspended media would be diluted at least 2500 times, resulting in a concentration of less than 0.04  $\mu$ g/mL. This is much lower than the MIC

ampicillin for *S. aureus*, which we measured as 0.25  $\mu$ g/mL (using broth microdilution in LB media), and is therefore unlikely to influence the properties of *S. aureus* when grown under mixed-species conditions.

## 2.7. Confocal microscopy and image acquisition

At 4, 8, 24, and 48 h, undisturbed *P. aeruginosa* and *S. aureus* mixed-species and single-species biomass in the 4-D microenvironment, in IVWM only or in LB medium were imaged using confocal laser scanning microscopy (Leica, Germany, LASX TCS SP). Briefly, each well was imaged at the approximate center, with at least 3 biological replicates for each time point. To visualize GFP-labeled *S. aureus*, a 488 nm excitation filter and 497 nm–542 nm emission filter was used. To visualize mCherry-labeled *P. aeruginosa*, a 561 nm excitation filter and 586 nm–656 nm emission filter was used. To visualize DAPI-stained host cell nuclei, a 405 nm excitation filter and 414 nm–485 nm emission filter was used. Biomass on fixed host cell scaffolds were imaged using a Z-stacks that started below the lower end of the biomass and up to 175  $\mu$  m thickness (above the upper end of the entire biomass), with a 5  $\mu$  m step size. For imaging the host cell scaffolds alone (without biofilms), Z-stacks of 1  $\mu$  m step size and 60  $\mu$  m total thickness were acquired, with two fields of view per well.

## 2.8. Image processing and analysis

Image analysis was done using open-source image analysis tools, ImageJ and BiofilmQ v0.2.1., with Paraview v5.10.0 used for rendering [45–52].

To characterize the host cell scaffolds, a four-step process with BiofilmQ v0.2.1 was used [45,46], consisting of image preparation, image processing, calculation of features of the nuclei and visualization. Briefly, each DAPI-stained image was subjected to separation using an intensity threshold filter to isolate individual nuclei. This calculated the total number of host cell nuclei in the visualized area. Each separated nucleus and its MATLAB parameter files were exported into a separate folder and processed independently for analysis. For image processing, each nucleus was subjected to semantic segmentation using the Otsu thresholding method [47]. Further, the images were subjected to de-noising by convolution (kernel size in pixels [xy,z]-5,3) and top-hat filter of size 25 vox (14.20  $\mu$  m) to remove background fluorescence. Next, object declumping by cube segmentation was used for dissection of each nuclei into smaller cubes (20 vox or 11.36  $\mu$  m). In addition, a small object removal filter was used to remove voxel clusters of size less than 5000 vox to refine the visualized area prior to parameter calculations. Local and global parameters in BiofilmQ v0.2.1 [45,46] were used for calculating height, shape-volume and base-area of the nuclei. During processing, visualizations were generated using the.vtk file output capability within BiofilmQ v0.2.1 [45,46] and rendered using the open-source tool Paraview v5.10.0 [48–50].

Aggregate sizes for *P. aeruginosa* and *S. aureus* in mixed-species and single-species biomass (in the 4-D microenvironment or in IVWM only or in LB medium) were estimated using ImageJ [51–53]. For this, the LIF files for each time point were imported into ImageJ and maximum intensity Z-projections of relevant channels were obtained. Otsu's automated thresholding method was applied to the Z-projection, and the areas of thresholded particles, representing aggregate sizes, were measured using the particle size analysis tool. Resulting aggregate size values were exported to a spreadsheet and grouped into the following aggregate size ranges for 4h: <5  $\mu$  m<sup>2</sup>, 5–10  $\mu$  m<sup>2</sup>, 10–20  $\mu$  m<sup>2</sup>, 20–50  $\mu$  m<sup>2</sup>, 50–100  $\mu$  m<sup>2</sup>, and >100  $\mu$  m<sup>2</sup>. For 8, 24 and 48 h time points, the aggregate sizes were grouped as <25  $\mu$  m<sup>2</sup>, 25–50  $\mu$  m<sup>2</sup>, 50–100  $\mu$  m<sup>2</sup>, 100–1000  $\mu$  m<sup>2</sup>, 1000–10000  $\mu$  m<sup>2</sup> and >10000  $\mu$  m<sup>2</sup>. Further, the percent count for each aggregate size range was calculated as the number of aggregates in a given size range/total number of aggregates x 100.

The thickness of *P. aeruginosa* and *S. aureus* biomass under mixed-

species or single-species conditions (in the 4-D microenvironment or in IVWM only or in LB medium) at relevant time points was measured using ImageJ [51,52]. Briefly, the side view projection images of the Z-stacks (of the relevant channel) were imported in ImageJ [51,52]. For a given replicate, the biomass boundary was defined manually using the polygon selection tool, and the thickness of the biomass was measured across every 25  $\mu\text{m}$  on the X-axis. The mean of the 23 measurements was considered the average thickness for the biomass replicate. The final mean thickness at each time point represents the average thickness of three biological replicates.

To measure the co-localization of mixed-species *P. aeruginosa* and *S. aureus* biomass with respect to each other (in the 4-D microenvironment or in IVWM only or in LB medium), the 3-D overlap parameter in BiofilmQ v0.2.1 was used [45,46]. This feature quantifies the volume overlap or co-localization of two fluorescent channels in a given space. A local parameter called 'Correlation Local3dOverlap' calculates the volume overlap in  $\mu\text{m}^3$  of each object in channel 3 (GFP-*S. aureus*) with all segmented objects in channel 4 (mCherry-*P. aeruginosa*), as well as the volume overlap of each object in channel 4 with all segmented objects in channel 3. This provides a 'Correlation LocalOverlapFraction', which is obtained by dividing 'Correlation Local3dOverlap' by the volume of the object. These values are then used to provide the user with a 3-D overlap fraction for the entire channel or the Biofilm\_OverlapFraction, defined as the sum of the Correlation LocalOverlapFraction for all objects in a specific fluorescence channel.

To quantify the spatial organization of *P. aeruginosa* and *S. aureus* in the mixed-species biomass (in the 4-D microenvironment or in IVWM only or in LB medium), LIF files containing images of mixed-species biofilms for each time point were imported into ImageJ [51,52], following which the entire Z-stack for each relevant channel was thresholded using Otsu's thresholding method. The mean gray value (MGV, indicative of fluorescent intensities) of the thresholded areas for each Z-slice in a given Z-stack was calculated using the 'measure stack' tool in ImageJ [51,52]. MGVs were normalized to the highest MGV in a given dataset, and plotted as a distribution of biomass over Z-thickness. Biomass distribution peak widths were calculated as the distance (in  $\mu\text{m}$ ) covered by >20% of the normalized MGV in a Z-stack; it is the difference between the X intercepts where the MGV is >20% of the highest value in the data set at the higher and lower ends of the Z-thickness.

Biomass composition of *P. aeruginosa* and *S. aureus* in mixed-species and single-species biofilms (in the 4-D microenvironment or in IVWM only or in LB medium) was calculated using MGV in ImageJ [51,52]. For this, LIF files for each time point were imported into ImageJ, and maximum intensity Z-projections of relevant channels were obtained, which were then subject to Otsu's automated thresholding method [47, 54]. MGVs were obtained for *P. aeruginosa* and *S. aureus* single-species biomass, as well as separately for *P. aeruginosa* and *S. aureus* in the mixed-species biomass, for each time point. The ratio of MGVs for *P. aeruginosa* to *S. aureus* in the mixed-species biomass, and for mixed-species to single-species biomass for *P. aeruginosa* to *S. aureus*, was obtained to analyze the composition of mixed-species biomass and possible role of interspecies interactions across time points.

## 2.9. Statistical analysis

Statistical analysis was performed using GraphPad Prism 6.01 for Windows (GraphPad Software, San Diego, California USA) [55]. A one-way or two-way ANOVA with Fisher's LSD test for multiple comparisons was performed and a p-value of  $\leq 0.05$  was considered significant.

## 3. Results and discussion

### 3.1. A 4-D wound microenvironment with host cell scaffolds and an *in vitro* wound milieu (IVWM) to study the structure and organization of mixed-species biofilms

The concept of the 4-D wound microenvironment is broadly based on *in vitro* cell culture techniques, classified as 2-D, 2.5-D and 3-D systems [56]. In contrast to conventional cell 2-D culture on flat surfaces, in 2.5-D cell culture, cells are grown on layers of extracellular matrix proteins (ECM) proteins [57,58]. However, 3-D cell culture systems take this further, with cells grown in or on artificial microenvironments (on scaffolds or scaffold-free), in interaction with each other and the environment [59]. A more recent concept, 4-D cell culture consists of 3-D cell culture systems with an additional dimension, such as biochemical or biophysical stimuli [60–64], that more closely recapitulate the microenvironment.

Recapitulating the infection microenvironment is particularly important in the context of biofilms in wounds where in contrast to standard laboratory studies on 2-D surfaces (Fig. 1A), biofilms are observed as bacterial aggregates, attached to the surface of, and surrounded by, the wound bed [5,7,65]. The wound bed is made up of host cells such as epidermal keratinocytes and dermal fibroblasts [37,44], and is bathed in protein-rich wound milieu, with a characteristic biochemical and nutrient profile [66,67]. Given this, biofilms in wounds form and exist in close approximation with the wound microenvironment [5–8]. Previous studies have aimed to recreate this complex microenvironment under laboratory conditions, with mixed-species biofilms grown on 3-D human skin epidermis constructs [32,68], with a focus on studying host inflammatory responses and effects of antimicrobial treatments.

To study the structure and organization of mixed-species biofilms in the wound microenvironment, we have developed an *in vitro* platform consisting of a 3-D reconstructed 'wound bed' and an *in vitro* wound milieu, which provides the fourth dimension that represents the biochemical and nutrient profile of the infection state; this set-up is together referred to as the 4-D wound microenvironment (Fig. 1B and C). The 'wound bed' was reconstructed using co-cultured HaCaT and HDFa cells, grown and fixed to form a confluent host cell scaffold. Based on our previous work, the *in vitro* wound milieu (IVWM) mimics the composition of clinical wound fluid, consisting of fetal bovine serum (FBS), with additional matrix and biochemical factors, such as collagen, fibrinogen, fibronectin, lactic acid and lactoferrin [35]. The IVWM was seen to support the growth of mixed-species biofilms of *P. aeruginosa* and *S. aureus*, and recapitulate key features such as biomass formation, metabolic activity and interspecies interactions [35].

In this study, we leveraged the 4-D wound microenvironment to study the structure of mixed-species *P. aeruginosa* and *S. aureus* biofilms across multiple levels of organization, such as aggregate dimensions and biomass thickness, species co-localization and organization within the biomass, biomass composition and interspecies interactions (Fig. 1D and E). To study the possible role of interspecies interactions, *P. aeruginosa* and *S. aureus* were also studied as single-species biofilms. Further, to study the individual roles of the host cell scaffold and IVWM in the 4-D microenvironment, and to compare with laboratory media conditions, mixed-species and single-species biofilms grown in IVWM and Luria-Bertani (LB) media were also analyzed.

### 3.2. 3-D features of the co-cultured host cell scaffolds with HaCaT + HDFa cells

In clinical wound biopsies, as well as *ex vivo* human skin wounds, the wound bed consists of keratinocytes and fibroblasts, with the two cell types in close association with each other [69–72]. Consequently, studies aiming to recapitulate the wound bed, include both fibroblasts and keratinocytes, with varying seeding and layering approaches [32,

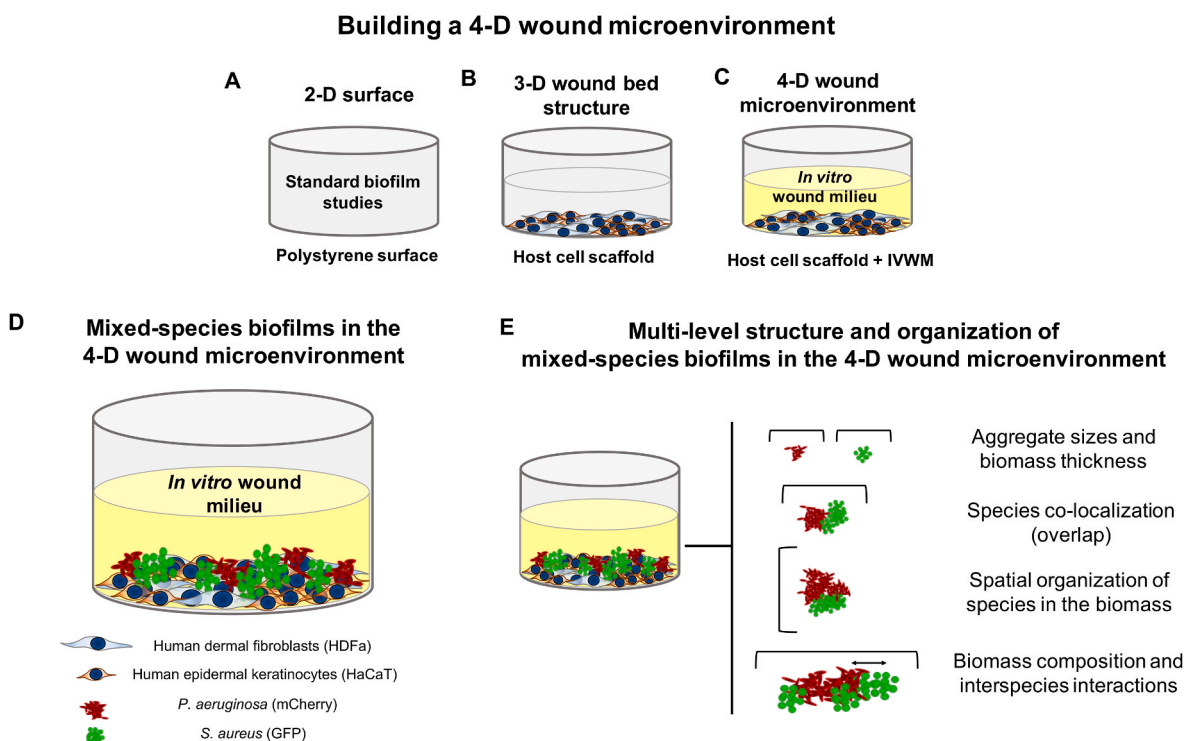


**Fig. 1.** Building a 4-D wound microenvironment consisting of mixed-species *P. aeruginosa* and *S. aureus* biofilms on a co-cultured host cell scaffold of epidermal keratinocytes and dermal fibroblasts, in the presence of an *in vitro* wound milieu. (A) Standard biofilm studies typically use 2-D polystyrene surfaces to grow and study biofilms. (B) Host cells, such as human dermal fibroblasts (HDFa) and epidermal keratinocytes (HaCaT), provide a 3-D surface that resembles the cellular composition and organization of the wound bed. (C) The IVWM recapitulates the composition of clinical wound fluid, with matrix and biochemical factors, and provides the additional dimension that represents the biochemical and nutrient profile of the infection state. (D) Mixed-species *P. aeruginosa* and *S. aureus* biofilms are grown in the 4-D microenvironment. (E) The 4-D microenvironment was leveraged to study the structure of mixed-species *P. aeruginosa* and *S. aureus* biofilms across multiple levels of organization.

44,73,74]. Notably, biofilms in wounds form and exist in the presence of host cellular elements [5–8]. To reconstruct the ‘wound bed’, HaCaT and HDFa cells were co-cultured to form 3-D host cell scaffolds, following which they were fixed and stained to visualize host cell nuclei. As seen in [Suppl Figure 1A](#), the co-cultured host cell scaffolds consist of both HaCaT and HDFa cells, with characteristic co-culture arrangements. HaCaT cells are observed as closely-packed clusters, surrounded by sheaths of dermal fibroblasts (HDFa), seen as large, flat, spindle-shaped cells with elongated protrusions (inset). This structure and arrangement resembles previous *ex vivo* and *in vitro* wound bed models [32,44,75], including reconstructed human skin models. The co-cultured scaffolds showed an average of  $\sim 140 \pm 20$  cells (both HaCaT and HDFa) in a visualized area of  $581.2 \times 581.2 \mu\text{m}$ , consisting of  $88 \pm 16$  HaCaT cells and  $52 \pm 4$  HDFa cells. This results in  $13000 \pm 1500$  cells in the well (culturable surface area of  $0.32 \times 10^8 \mu\text{m}^2$ ;  $n = 2$ , two biological replicates with two fields of view per well, error represents SEM), which based on the average cell area for HaCaT and HDFa cells ( $3000 \mu\text{m}^2$  and  $4000 \mu\text{m}^2$ ) respectively [76–79], corresponds to a coverage of close to 100% of the well surface [80,81].

To characterize the 3-D features of the co-cultured scaffolds, BiofilmQ v0.2.1 [45,46] was used to analyze the height, shape-volume and base-area of the host cell nuclei ( $n = 2$ , biological replicates with two fields of view per well). The average height of the HaCaT nuclei measured  $13.2 \pm 0.5 \mu\text{m}$  and that of the HDFa nuclei measured  $13.2 \pm 0.6 \mu\text{m}$  ([Suppl Figure 1B](#)). It is important to note that the cytoplasmic layer surrounding the nucleus, typically  $15\text{--}30 \mu\text{m}$  [82–84], would further add to the thickness of the substratum. The base-area of the nucleus represents the surface area occupied in the horizontal plane, and the shape-volume represents the volume occupied by the nucleus across both horizontal and vertical planes. Given that nuclear morphology varies with cell shape, and nuclear volume positively correlates with cell

volume [85–87], base-area and shape-volume can serve as proxies for heterogeneity in cell shape and volume. As seen in [Suppl Fig. 1C and D](#), in the co-cultured HaCaT + HDFa scaffolds, host cell nuclei for each cell type showed varied distribution with respect to base-area and shape-volume, in addition to variation across the two cell types. Taken together, the co-cultured host cell scaffolds consist of a confluent layer of fixed HDFa and HaCaT cells, with 3-D features that resemble the cellular composition and organization of the wound bed.

### 3.3. Mixed-species and single-species *P. aeruginosa* and *S. aureus* biofilms in the 4-D microenvironment, in comparison with IVWM only and LB medium

To study mixed-species biofilms in the 4-D microenvironment, IVWM only and LB medium *P. aeruginosa* and *S. aureus* were mixed in the IVWM or LB medium, and seeded together (in a 1:1 ratio) on the HaCaT + HDFa fixed host cell scaffolds (or without scaffolds in the case of IVWM only and LB medium), followed by incubation at  $37^\circ\text{C}$  and imaging at 4, 8, 24 and 48 h. For comparison with single-species biofilms, *P. aeruginosa* and *S. aureus* were mixed separately in the IVWM or LB medium, and seeded alone with or without host cell scaffolds.

As seen in [Fig. 2A](#), in the 4-D wound microenvironment, *P. aeruginosa* and *S. aureus* co-exist under mixed-species conditions, with the structure and organization of the biomass observed to vary across time points. At 4 h, *P. aeruginosa* and *S. aureus* are seen as bacterial aggregates, in close approximation with, and dispersed across, the host cell scaffold (seen as DAPI-stained nuclei). Across subsequent time points of 8, 24 and 48 h, *P. aeruginosa* is observed to grow into dense, mat-like biofilms, whereas *S. aureus* retains its aggregate structure and is observed to be progressively enmeshed in the dense, mat-like growth of *P. aeruginosa* ([Fig. 2A](#)). Overall, this resembles the presence and growth of biofilms in clinical

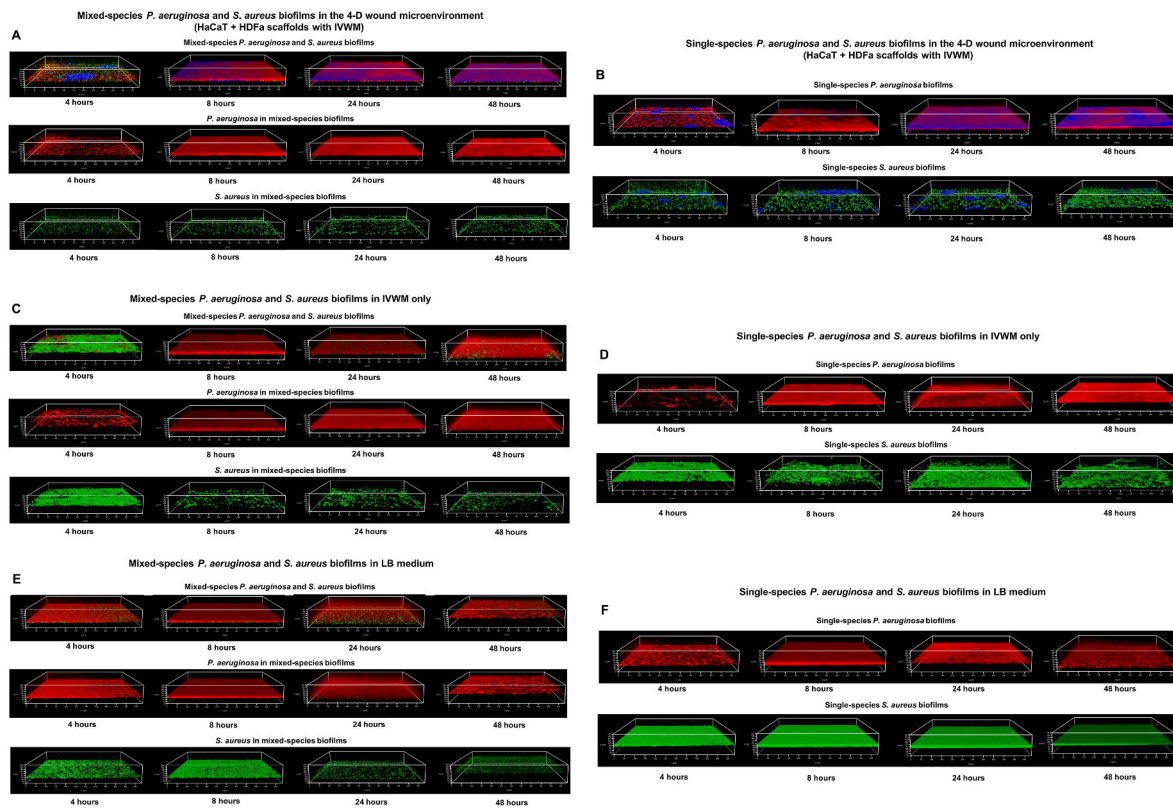


**Fig. 2.** Mixed-species and single-species biomass of *P. aeruginosa* and *S. aureus* biofilms in the 4-D microenvironment, IVWM only and LB medium, showing distinct structure and organization. *P. aeruginosa* (PAO1-pUCP18, mCherry) and *S. aureus* (Strain AH 133-pAH13, GFP) were seeded in a 1:1 ratio in IVWM or LB on fixed host cell scaffolds (or without scaffolds). Following incubation at 37 °C, the mixed-species biomass was imaged at 4, 8, 24 and 48 h. Representative images of mixed-species and single-species *P. aeruginosa* and *S. aureus* biomass across time points in (A–B) the 4-D microenvironment, (C–D) IVWM only, and (E–F) LB medium. The blue stain represents the DAPI-stained host cell nuclei; the diffusion of the stain is likely due to the destruction of host cell structure with bacterial growth. (For interpretation of the references to colour in this figure legend, the reader is referred to the Web version of this article.)

wounds, as well as previous *in vitro* host cell-biofilm models [6,7,13]. Further, *P. aeruginosa* aggregates in wounds are typically observed to be large and dense, extending across the wound surface area [6,88]. This is in contrast to *S. aureus* aggregates, which are most often seen as small and discrete clumps [6,7]. Notably, the visualized biomass consists of bacteria in discrete aggregates, larger mats, as well as planktonic cells. In doing so, it resembles the structural complexity of biofilms in wounds, where bacteria can be seen as aggregates and dense clumps, as well as planktonic cells [9]. Notably, this distinct structural organization of *P. aeruginosa* and *S. aureus* is also seen under single-species conditions (Fig. 2B). It is important to note that biomass accumulation at later time points, is likely leading to the progressive destruction of the host cell scaffold, seen as loss of nuclear structure and diffusion of the nuclear stain (DAPI) (Fig. 2A and B, Suppl Figure 2).

For mixed-species biofilms in IVWM only and LB medium, *P. aeruginosa* biomass across time points is seen to form dense mats, similar to that in the 4-D microenvironment (also seen under single-species conditions) (Fig. 2C–F). On the other hand, for *S. aureus* under mixed-species conditions in the IVWM only (as compared with the 4-D microenvironment) denser aggregate structures are seen at 4 h, with smaller, more discrete aggregates at later time points (Fig. 2C). This is distinct from that observed under single-species conditions, where *S. aureus* is seen as dense biomass across time points (Fig. 2D). The formation and development of *S. aureus* in mixed-species biofilms is also distinct in LB medium, showing dense aggregates at early time points, followed by sparse biomass at 24 and 48 h (Fig. 2E). However, under single-species conditions in LB medium, *S. aureus* is seen as dense mats of biomass across early and subsequent time points (Fig. 2F). This decline of *S. aureus* biomass under mixed-species conditions, likely points to the

effect of interspecies interactions in LB medium.

Taken together, mixed-species *P. aeruginosa* and *S. aureus* biofilms in the 4-D microenvironment show characteristic structure and organization, with notable differences from observations in the IVWM only and LB medium, as well as across mixed-species and single-species biomass under the different conditions. This underscores the possible roles of the host cell substratum and biochemical milieu, alone and together, in influencing the structure of early biofilm aggregates, formation of subsequent dense biofilms and co-existence of the two bacterial species. Given this, the 4-D platform provides a relevant and tractable system to study the structure of mixed-species biofilms across multiple levels of organization, and in comparison with IVWM only and LB medium can provide insights into the specific roles of the host cell substratum, biochemical milieu and interspecies interactions in the recapitulated microenvironment.

### 3.4. Aggregate dimensions and biomass thickness of *P. aeruginosa* and *S. aureus* mixed-species biofilms in the 4-D wound microenvironment, in comparison with IVWM only and LB medium

Aggregate sizes for *P. aeruginosa* and *S. aureus* in mixed-species and single-species biofilms at relevant time points in the 4-D microenvironment, IVWM only and LB medium, were measured using the particle size analysis tool in ImageJ [51–53]. It is important to note that while biofilm aggregates are 3-D structures, we measured the size of the aggregates in area ( $\mu\text{m}^2$ ), which is in accordance with previous studies [89]. Further, the biomass thickness of *P. aeruginosa* and *S. aureus* in mixed-species and single-species biofilms at relevant time points was measured using ImageJ [51,52].

As seen in Fig. 3A, early biofilms (at 4 h) of *P. aeruginosa* and *S. aureus* under mixed-species conditions, consist of a majority of single bacterial cells or small aggregates (<5  $\mu\text{m}^2$ ) that constitute ~76% and ~82% of the total biomass respectively. The next largest group of aggregates for both species are in the 5–10  $\mu\text{m}^2$  size range, representing ~11% and ~8% of the aggregate size distribution for *P. aeruginosa* and *S. aureus* respectively. This is followed by larger aggregates in the 10–20  $\mu\text{m}^2$  size range, that comprise ~5–6% of the total biomass. Taken together, the early mixed-species biofilm consists of ~80–90% of smaller aggregates of less than 10  $\mu\text{m}^2$  size, with larger aggregates (20–50  $\mu\text{m}^2$ , 50–100  $\mu\text{m}^2$  and >100  $\mu\text{m}^2$  in size) comprising ~10–20% of the total biomass; *S. aureus* biomass consists of a significantly larger number of smaller aggregates, and *P. aeruginosa* shows a shift towards larger aggregate sizes (Fig. 3A, Suppl Tables 1 and 2). This corresponds to the well-studied model of biofilm development, where biofilms are typically seeded by single cells (planktonic) or small aggregates [29]. Further, the aggregate sizes in the 4-D microenvironment correspond to aggregate sizes measured in clinical wounds, including at the wound edges where keratinocytes and fibroblasts are found in close proximity [90,91]. It is important to note that while biofilms were seeded from bacterial cultures grown under planktonic conditions, overnight bacterial suspensions are known to contain a mixture of single cells and pre-formed aggregates [29,92–94]. This could contribute to a variation in the initial seeding of aggregates, and thereby influence subsequent aggregate sizes, including the growth of a few large aggregates [29]. At 8 h, *S. aureus* biomass consists of a majority of aggregates (~94%) in the size range of <25  $\mu\text{m}^2$ . This proportion was observed to significantly decline at 24 and 48 h, with ~80% of aggregates in the size range of <25  $\mu\text{m}^2$ , and a shift towards larger aggregate sizes in the range of 25–50  $\mu\text{m}^2$  and 50–100  $\mu\text{m}^2$  (~11–12%) (Fig. 3B). For *P. aeruginosa*, across 8, 24 and 48 h, the biomass grew into thick mats, measuring  $56 \pm 3 \mu\text{m}$  at 8 h, and  $46 \pm 1 \mu\text{m}$  and  $44 \pm 4 \mu\text{m}$  at 24 and 48 h respectively (Fig. 3C). When compared with single-species biofilms in the 4-D microenvironment, the overall aggregate size distributions for *P. aeruginosa* and *S. aureus* are

similar across time points, with the biomass of both species consisting of a majority of small aggregates and *P. aeruginosa* growing to form dense mats (Fig. 3D–F, Suppl Tables 1 and 2).

In the IVWM only, while the overall aggregate size distributions for *P. aeruginosa* in the mixed-species biomass is similar to that in the 4-D microenvironment, for *S. aureus* at 4 h, there is a shift in aggregate sizes towards larger aggregates in 5–10  $\mu\text{m}^2$  (~8% in the 4-D microenvironment versus ~13% in IVWM only) and 10–20  $\mu\text{m}^2$  size ranges (~5% in the 4-D microenvironment versus ~9% in IVWM only) (Fig. 3G, Suppl Tables 1–4). This indicates that in the presence of the biochemical milieu alone, *S. aureus* forms larger aggregates, which possibly highlights the role of host cell substratum in influencing the initial attachment and early aggregation of *S. aureus*. In addition, host matrix components such as fibrinogen and fibronectin (present in the IVWM) are known to influence the aggregation of *S. aureus*, including observations of large aggregates coated with fibrinogen [95,96].

On the other hand, across the later time points of 24 and 48 h, in mixed-species biomass in IVWM only, *S. aureus* biomass shows a shift towards larger numbers of smaller aggregates in the <25  $\mu\text{m}^2$  size range (~89% each at both time points), as compared with that in the 4-D microenvironment (~80% each at both time points) (Fig. 3H). This suggests that during subsequent biomass development, *S. aureus* forms larger aggregates in the presence of the host cell substratum, as compared with when in the biochemical milieu alone. This could possibly be due to differences in growth properties and features of biofilm aggregates when attached to a cellular substratum, as opposed to when grown in the biochemical milieu [97,98]. In the IVWM only, single-species *S. aureus* biomass also shows a significant shift to smaller aggregates at later time points (~97% and ~94% at 24 and 48 h) (Fig. 3J and K, Suppl Tables 3–4). Further, in the absence of the host substratum and milieu (as in LB medium), smaller aggregates constitute the majority of the biomass (>99% in the <25  $\mu\text{m}^2$  size range), an effect in stark contrast to the dense mats seen when *S. aureus* is grown in single-species conditions (Fig. 3M–Q, Suppl Tables 5–6). Notably, this underscores the

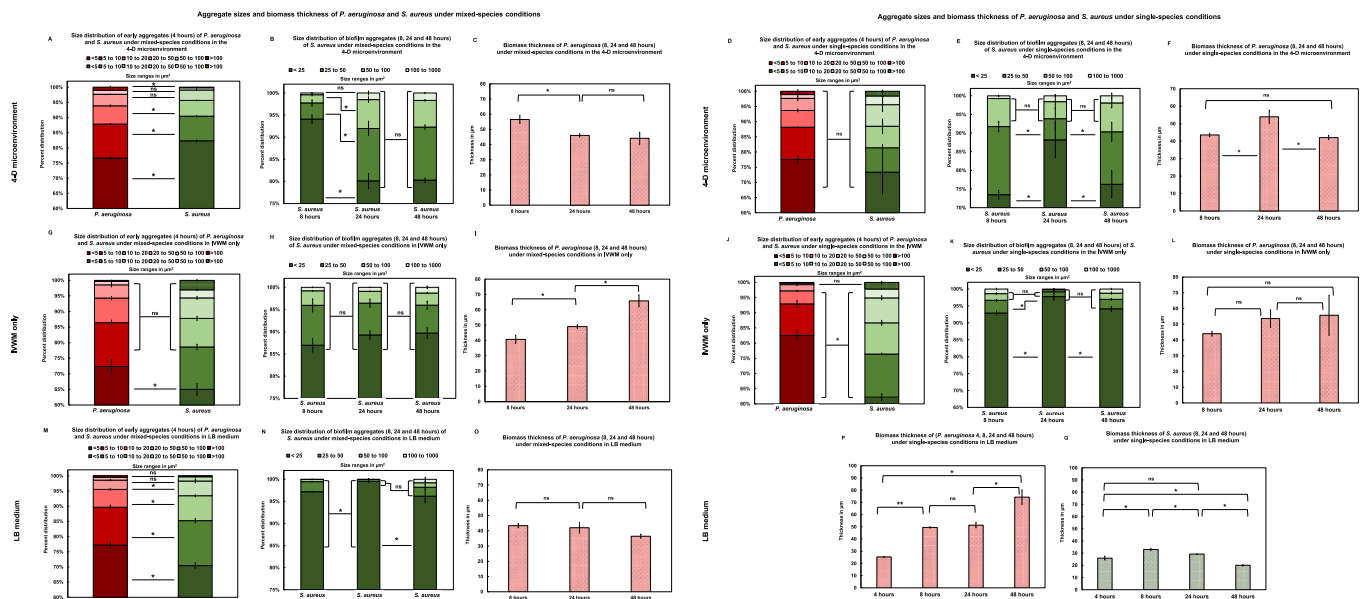


**Fig. 3. Aggregate size distribution and biomass thickness of *P. aeruginosa* and *S. aureus* under mixed-species and single-species conditions in the 4-D microenvironment, IVWM only and LB medium.** Aggregate sizes for *P. aeruginosa* and *S. aureus* in mixed-species and single-species biomass were measured using the particle size analysis tool in ImageJ [51,52]. Biomass thickness for *P. aeruginosa* and *S. aureus* in mixed-species and single-species biomass was measured using the side view projection images of the Z-stacks in ImageJ [51,52]. Aggregate size distribution and biomass thickness of *P. aeruginosa* (shades of red or red lines) and *S. aureus* (shades of green or green lines) under mixed-species and single-species conditions in (A–F) the 4-D microenvironment, (G–L) IVWM only, and (M–Q) LB medium. At 4 h, the aggregate size ranges shown are <5  $\mu\text{m}^2$ , 5–10  $\mu\text{m}^2$ , 10–20  $\mu\text{m}^2$ , 20–40  $\mu\text{m}^2$ , 50–100  $\mu\text{m}^2$  and >100  $\mu\text{m}^2$ , and at 8, 24 and 48 h, size ranges shown are <25  $\mu\text{m}^2$ , 25–50  $\mu\text{m}^2$ , 50–100  $\mu\text{m}^2$  and 100–1000  $\mu\text{m}^2$ . For *P. aeruginosa* and *S. aureus* biomass observed as dense mats, biomass thickness was measured ( $\mu\text{m}$ ). Error bars represent SEM,  $n = 3$ , biological replicates; ns indicates no significant difference, a  $p$ -value  $\leq 0.05$  was considered significant (\*). (For interpretation of the references to colour in this figure legend, the reader is referred to the Web version of this article.)

role of interspecies interactions in influencing aggregate features and formation during biomass development. In the IVWM only and LB medium, *P. aeruginosa* grew to form dense mats at 8, 24 and 48 h, under both mixed-species and single-species conditions (Fig. 3I, O, L and P).

Taken together, in the 4-D microenvironment, early aggregate features of *P. aeruginosa* and *S. aureus* mixed-species biomass are largely influenced by the presence of the host substratum, whereas subsequent aggregate and biomass formation is likely influenced by an interplay between the host substratum, biochemical milieu and interspecies interactions.

### 3.5. Co-localization of *P. aeruginosa* and *S. aureus* in mixed-species biofilms in the 4-D wound microenvironment, in comparison with IVWM only and LB medium

To determine the co-localization of *P. aeruginosa* and *S. aureus* in the mixed species biomass in the 4-D microenvironment, IVWM only and LB medium, the 3D overlap analysis module of BiofilmQ v0.2.1 was used [45,46]. This tool measures the volumetric overlap fraction for each species, which is the volume of the species (channel) overlap in relation to the biomass of that species.

As seen in Fig. 4A, in the 4-D microenvironment at 4 h, a very small

fraction of the total biomass of *P. aeruginosa* was observed to overlap with *S. aureus*, with the non-overlapping fraction measuring ~99%. This could be due to the dispersed nature of the *P. aeruginosa* and *S. aureus* biomass, seen as discrete aggregates, under mixed-species conditions (Figs. 2 and 3). The *P. aeruginosa* overlap fraction increases across the time points of 8, 24 and 48 h, but continues to remain a very small fraction of the total *P. aeruginosa* biomass, accounting for ~2% of the species biomass at 48 h. This is possibly due to the growth of *P. aeruginosa* into thick, mat-like biofilms across time, resulting in small regions of overlap with *S. aureus* aggregates. On the other hand, for *S. aureus*, the biomass overlapping with *P. aeruginosa* at 4 h constitutes ~28% of the total *S. aureus* biomass (Fig. 4B). The larger overlap fraction of *S. aureus* with *P. aeruginosa*, as compared with vice-versa, could be due to the larger proportion of smaller aggregates in the *S. aureus* in the early mixed-species biomass (Figs. 2 and 3). At 8 h, the overlap fraction of *S. aureus* was observed to decrease to ~7%, followed by an increase across 24 and 48 h (~30% and ~28% respectively). This decrease in the *S. aureus* overlap fraction at 8 h could result from a combination of several factors such as growth and density of aggregates of *S. aureus* (bacteria in the center of the *S. aureus* aggregates would be considered as part of the non-overlap fraction), as well as increase in *P. aeruginosa* biomass.

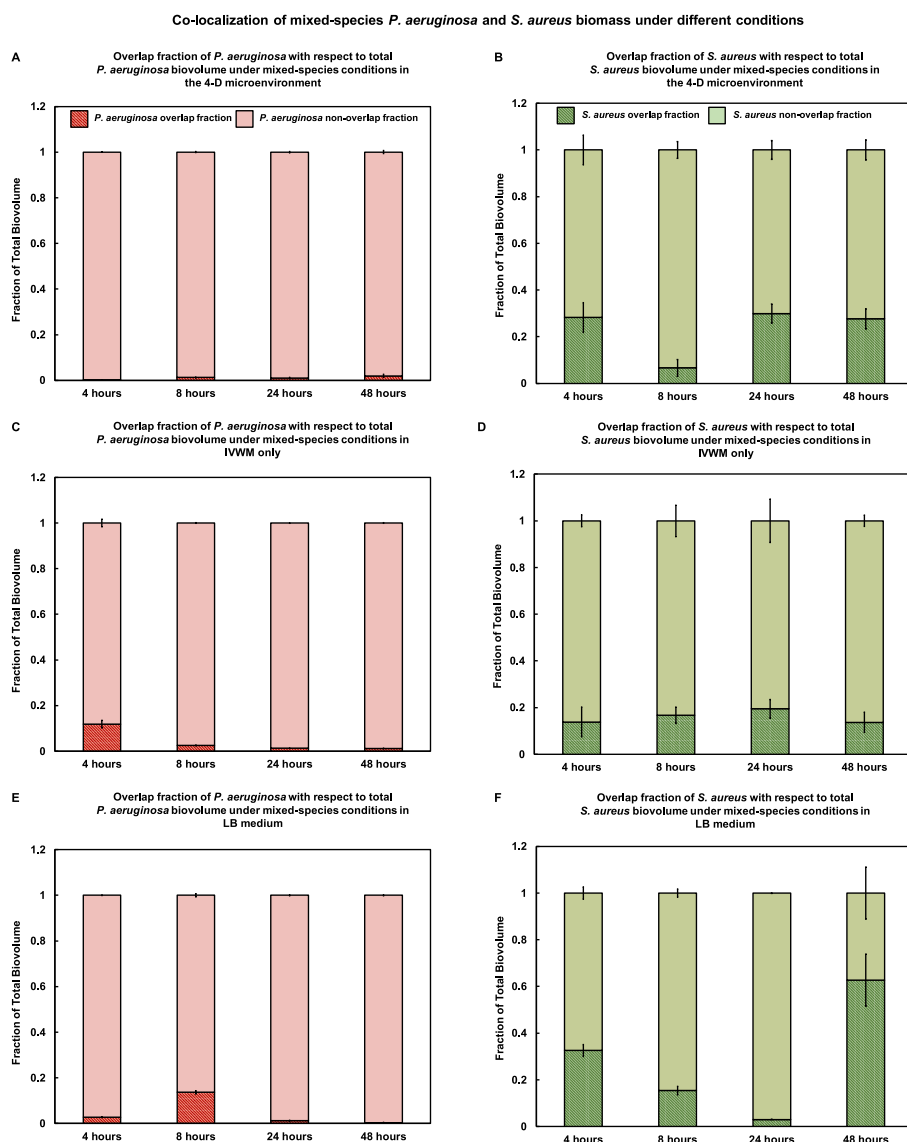


**Fig. 4.** Co-localization of *P. aeruginosa* and *S. aureus* biomass under mixed-species conditions in the 4-D microenvironment, IVWM only and LB medium. The co-localization of *P. aeruginosa* and *S. aureus* biomass with respect to the total biomass of the species was measured using the 3D overlap parameter in BiofilmQ v0.2.1 [45,46]. The overlap fraction of *P. aeruginosa* with respect to the total *P. aeruginosa* biovolume (solid red and red lines) and *S. aureus* (solid green and green lines) with respect to the total *S. aureus* biovolume in (A–B) the 4-D microenvironment, (C–D) IVWM only, and (E–F) LB medium. Error bars represent SEM, n = 3, biological replicates. (For interpretation of the references to colour in this figure legend, the reader is referred to the Web version of this article.)

In the IVWM only, the overall co-localization patterns are similar to that in the 4-D microenvironment, however a higher fraction of the total biomass of *P. aeruginosa* is seen overlapping with *S. aureus* at 4 h (~11%) (Fig. 4C–D). This is possibly due to the shift towards larger aggregates seen in *S. aureus* in IVWM only (Fig. 3), while the aggregate size distributions of *P. aeruginosa* remain similar across the 4-D microenvironment and IVWM only.

In LB medium, while *P. aeruginosa* continues to show a small fraction of overlap with *S. aureus*, whereas for *S. aureus* the overlap fraction with *P. aeruginosa* increases significantly at 48 h (Fig. 4E–F). This effect is likely due to interspecies interactions in LB medium, with the growth of *P. aeruginosa* resulting in destruction of *S. aureus* biomass, visibly evident as the majority of small *S. aureus* aggregates and the vertical displacement of residual biomass (Figs. 2 and 3).

Taken together, in the 4-D microenvironment in mixed-species conditions, *P. aeruginosa* and *S. aureus* co-exist in close proximity across time points, and the differences in overlap fractions between the two species indicates distinct spatial organization in the biomass.

### 3.6. Spatial organization of *P. aeruginosa* and *S. aureus* in mixed-species biofilms in the 4-D wound microenvironment, in comparison with IVWM only and LB medium

To study the spatial organization of *P. aeruginosa* and *S. aureus* in the mixed-species biomass in the 4-D microenvironment, IVWM only and LB medium, the MGV for each Z-slice in a given channel was calculated using the ‘measure stack’ tool in ImageJ [51,52]. MGVs were normalized to the highest MGV in a given dataset, and plotted as a distribution of biomass over Z-thickness and biomass distribution peak widths.

As seen in Fig. 5A, in the 4-D microenvironment at 4 h, the normalized MGV distribution of both *P. aeruginosa* and *S. aureus* in the mixed-species biomass is observed to coincide with that of the host cell scaffold (the DAPI channel) at the lower end of the Z-stack. At 8 h, the

normalized MGV distribution (Fig. 5B) shows the *P. aeruginosa* biomass to be distributed across a wider region as compared with *S. aureus*, with the *S. aureus* biomass observed in the lower regions of the biomass distribution. This is prominently observed at 24 and 48 h as well, with *P. aeruginosa* biomass is distributed across a wider thickness while *S. aureus* biomass is seen within the *P. aeruginosa* biomass (Fig. 5C and D).

Similar to that in the 4-D microenvironment, in IVWM only, at early time points, *P. aeruginosa* and *S. aureus* are well-mixed, which is followed by spatial organization of *S. aureus* in the lower regions of the mixed-species biomass (Figures E–H). On the other hand, in LB medium, while early mixed biomass shows spatial overlap between the two species, at later time points, the organization is distinct from that observed in both, the 4-D microenvironment and IVWM only. At 24 h, *S. aureus* is seen in the lower regions of the biomass, with a vertical displacement of *P. aeruginosa*, whereas at 48 h, both species show a vertical displacement, with dispersed biomass (Figures I–L).

The spatial re-organization seen across time points, in all three conditions, is also evident with biomass distribution peak widths (Figures M–O). In the 4-D microenvironment and IVWM only, the differences in the biomass peak widths between *P. aeruginosa* and *S. aureus* increase from 4 h to 48 h, with *P. aeruginosa* showing a larger distribution (at 48 h in the 4-D microenvironment, biomass distribution peak width for *P. aeruginosa* is ~77  $\mu\text{m}$  and for *S. aureus* ~32  $\mu\text{m}$ ). In LB medium, the differences in the biomass peak widths of the two species increase to show a significant difference from 4 h to 24 h (at 24 h biomass distribution peak width for *P. aeruginosa* is ~162  $\mu\text{m}$  and for *S. aureus* ~18  $\mu\text{m}$ ), which is followed by a marked increase in *S. aureus* distribution at 48 h (peak width ~77  $\mu\text{m}$ ). The growth of *P. aeruginosa* into dense, mat-like biofilms (Figs. 2 and 3), and possible inhibitory effect of *P. aeruginosa* on *S. aureus*, could result in the dispersal of *S. aureus* biomass.

Taken together, the 4-D microenvironment, the co-existing biomass

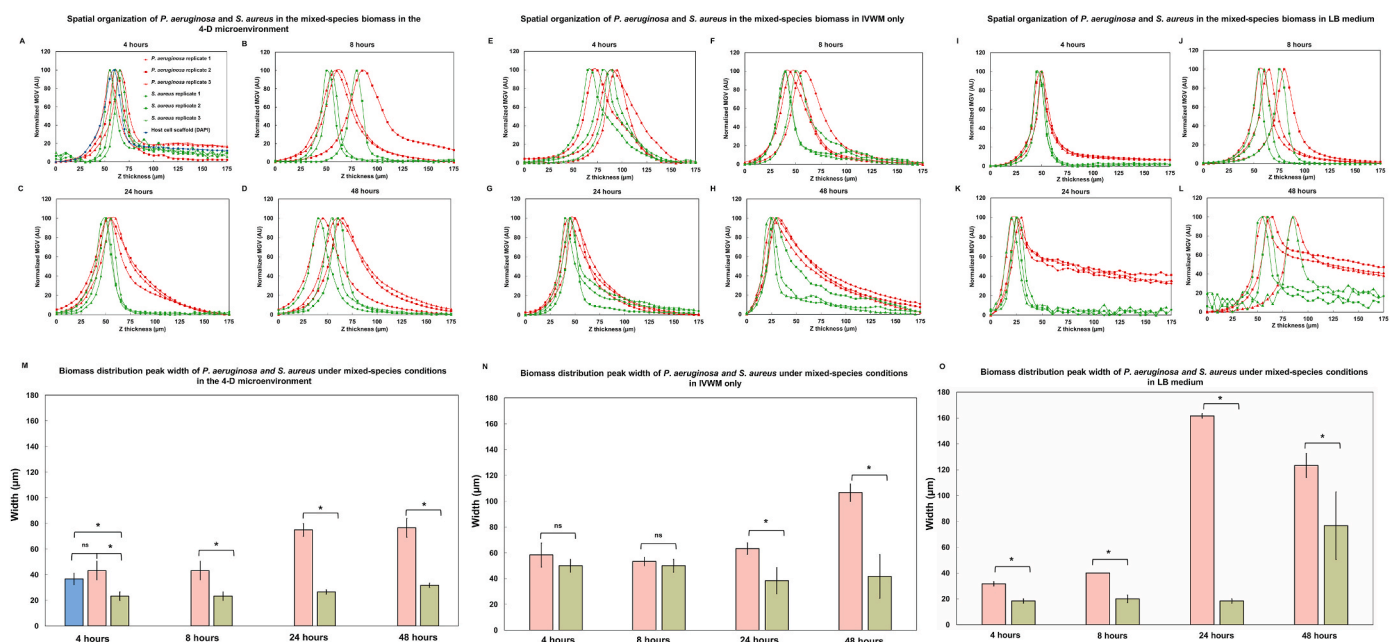


**Fig. 5. Spatial organization of *P. aeruginosa* and *S. aureus* under mixed-species conditions in the 4-D microenvironment, IVWM only and LB medium.** For *P. aeruginosa* and *S. aureus* in mixed-species biofilms, the MGV for each Z-slice in a given channel was calculated using ImageJ [51,52]. MGVs were normalized to the highest MGV in a given dataset, and plotted as a distribution of biomass over Z-thickness and biomass distribution peak widths. Spatial organization of *P. aeruginosa* and *S. aureus* under mixed-species conditions across time points in (A–D) the 4-D microenvironment, (E–H) IVWM only, and (I–L) LB medium. Each set of biological replicates for *P. aeruginosa* and *S. aureus* have been shown separately. (M–O) Biomass distribution peak widths of *P. aeruginosa* (red) and *S. aureus* (green) under mixed-species conditions in the 4-D microenvironment, IVWM only and LB medium. Error bars represent SEM,  $n = 3$ , biological replicates; ns indicates no significant difference, a  $p$ -value  $\leq 0.05$  was considered significant (\*). (For interpretation of the references to colour in this figure legend, the reader is referred to the Web version of this article.)

of *P. aeruginosa* and *S. aureus* (aggregates, mats and planktonic cells) undergo spatial reorganization across time points, with *S. aureus* segregating in the lower regions of the *P. aeruginosa* biomass. This distinct spatial reorganization is also observed in the IVWM only, as well as across later time points (mixed-species biomass is seen to destroy the host cell scaffolds over time), which possibly points to the role of the biochemical milieu in this effect. As part of future work, it would be interesting to understand the factors influencing the tendency of *S. aureus* to remain in the lower regions of the biomass, such as adhesion to the host cell scaffold at early time points, the role of specific components of the IVWM or interspecies interactions.

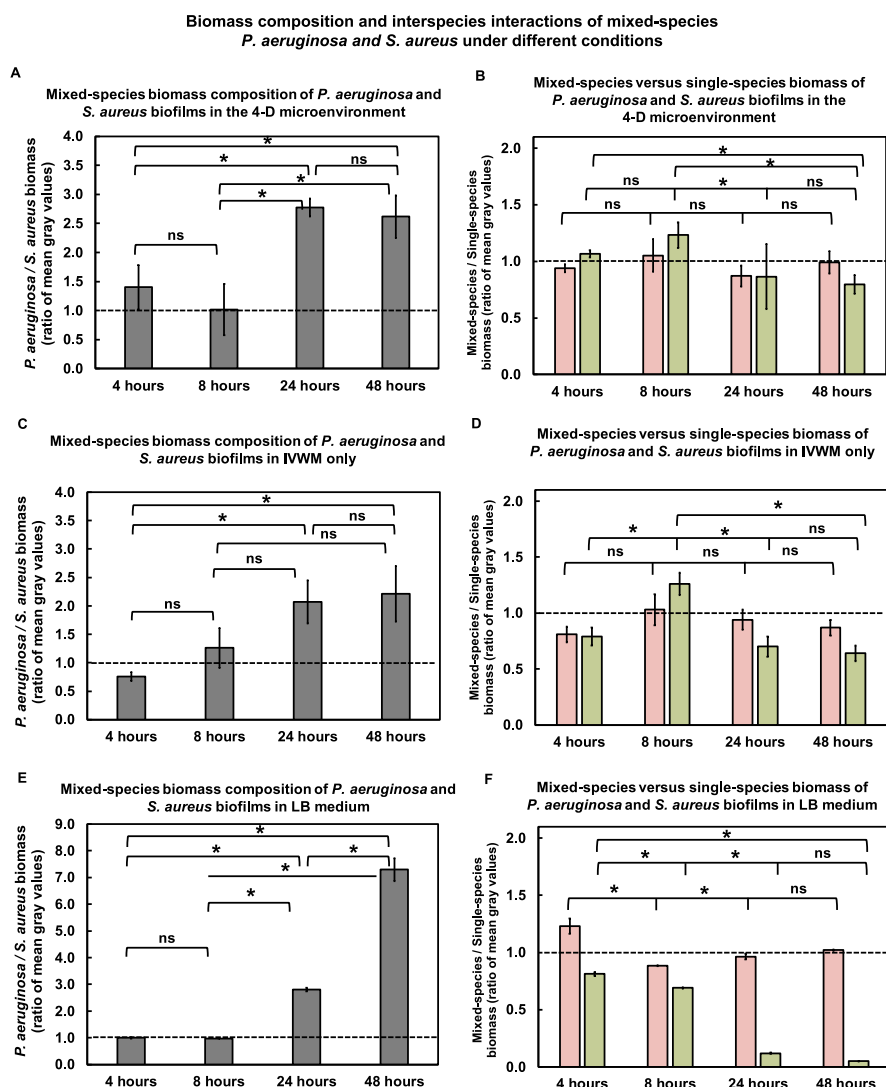
**3.7. Biomass composition of, and interspecies interactions between, *P. aeruginosa* and *S. aureus* in mixed-species conditions in the 4-D wound microenvironment, and in comparison with IVWM only and LB medium**

Biomass for mixed-species *P. aeruginosa* and *S. aureus* biofilms in the 4-D microenvironment, IVWM only and LB medium, was measured using MGV in ImageJ [51,52]. An MGV ratio of >1 represents more *P. aeruginosa* biomass and <1 represents more *S. aureus* biomass. To study the roles of the interspecies interactions, we compared the MGV ratio for *P. aeruginosa* and *S. aureus* under mixed-species to single-species conditions, with a ratio of 1 representing equal biomass for a species across both conditions, >1 represents more biomass for that species in

mixed-species conditions, and <1 represents more biomass in single-species conditions.

As seen in Fig. 6A, in the 4-D microenvironment, the ratio of the biomass of *P. aeruginosa* to *S. aureus* under mixed-species conditions increases from 4 h to 48 h, indicating a higher relative biomass of *P. aeruginosa* across time points. At 4 h, the ratio of the relative biomass of *P. aeruginosa* to *S. aureus* indicates nearly equal composition of both species, whereas across 24 and 48 h, the ratio of the relative biomass of *P. aeruginosa* which is more than twice that of *S. aureus* in the mixed-species biofilm. In Fig. 6B, the ratio of mixed-species to single-species biomass for *P. aeruginosa* in the 4-D microenvironment remains close to 1, with no significant difference across time points. On the other hand, for *S. aureus*, the ratio shows a significant decrease across 8 and 48 h. This indicates that while the 4-D microenvironment supports the mixed-species co-existence of *P. aeruginosa* and *S. aureus*, the growth of *S. aureus* is slightly impaired or inhibited. This could be due to interspecies interactions such as the active killing or inhibition of *S. aureus* by *P. aeruginosa* exoproducts (such as the *lasB* elastase) [21,99], which correlates with the increased accumulation of *P. aeruginosa* across time. At early time points, the possible inhibitory effect on *S. aureus* can be observed in the shift towards larger aggregate sizes under single-species conditions (absence of *P. aeruginosa*) (Fig. 3); at 8 h this is seen as an increase in aggregates in the 25–50 μm<sup>2</sup> and 50–100 μm<sup>2</sup> size ranges in the single-species biomass (Suppl Table 1). However, *P. aeruginosa* in

**Fig. 6. Biomass composition and interspecies interactions of *P. aeruginosa* and *S. aureus* under mixed-species conditions in the 4-D microenvironment, IVWM only and LB medium.** Biomass for *P. aeruginosa* and *S. aureus* biofilms, grown alone or together was measured using mean gray values (MGV) in ImageJ [51,52]. Ratio of *P. aeruginosa* to *S. aureus* in the mixed-species biomass, and ratio of mixed-species to single-species biomass for *P. aeruginosa* (red) and *S. aureus* (green) across 4, 8, 24 and 48 h in (A–B) the 4-D microenvironment, (C–D) IVWM only, and (E–F) LB medium. Error bars represent SEM, n ≥ 3, biological replicates; ns indicates no significant difference, a p-value ≤ 0.05 was considered significant (\*). (For interpretation of the references to colour in this figure legend, the reader is referred to the Web version of this article.)



single-species biomass grows into thick mats, similar to that in mixed-species conditions (Figs. 2 and 3).

The overall biomass composition and evidence of the marginal inhibitory effect of *P. aeruginosa* on *S. aureus* is also observed in the IVWM only, with a decline in *S. aureus* biomass across 8 and 48 h (Fig. 6C and D). This points to the predominant role of the biochemical milieu in the coexistence of both species and relative higher biomass of *P. aeruginosa*. This is further underscored by observations in LB medium, where *P. aeruginosa* is seen to significantly outcompete *S. aureus*; at 4 h, the ratio of the relative biomass of *P. aeruginosa* to *S. aureus* indicates nearly equal composition of both species, which increases 8-fold at 48 h. Further, the ratio of mixed-species to single-species biomass shows a marked decline in *S. aureus* across time points (Fig. 6E and F), which is very likely due to the well-studied effect of *P. aeruginosa* killing or inhibiting *S. aureus* in LB medium [18,35].

Taken together, the 4-D microenvironment supports the co-existence of *P. aeruginosa* and *S. aureus* in mixed-species biofilms, with a relative predominance of *P. aeruginosa*. This aligns with previous *in vivo* and clinical observations of wound biofilms [6,7,18,23,35,100], as well as biomimetic *in vitro* studies, where *P. aeruginosa* and *S. aureus* co-exist in wound-like conditions, however *P. aeruginosa* is found in larger numbers [18,35]. This is possibly due to the inhibitory effect of *P. aeruginosa* on the growth of *S. aureus* (widely observed under *in vitro* conditions) [18, 21,99], but could also be due to a combination of factors, including the increased growth of *P. aeruginosa* under mixed-species conditions [23].

### 3.8. Proposed fine-tuned model of the structure and organization of mixed-species *P. aeruginosa* and *S. aureus* biomass in the wound bed

In this study, the 4-D wound microenvironment, with co-cultured (fixed) HaCaT + HDFa scaffolds and IVWM, recapitulates the co-existence and interactions of *P. aeruginosa* and *S. aureus* in the presence of host and matrix elements (Fig. 7). Based on our findings, under these wound-like conditions, *P. aeruginosa* and *S. aureus* grow to form mixed-species biomass with distinct structure and organization, with *S. aureus* observed as discrete aggregates and *P. aeruginosa* growing to form dense, mat-like biofilms. In early mixed-species conditions, *P. aeruginosa* and *S. aureus* are seen as biofilm aggregates or planktonic cells close association with the host cell scaffold, with the nearly equal presence of both *P. aeruginosa* and *S. aureus*. At this stage, *P. aeruginosa* is seen to form larger aggregates as compared with *S. aureus*, which could

possibly influence the subsequent organization and growth of the species in the biomass. In subsequent growth of the mixed-species biomass, *S. aureus* was observed to retain its aggregate structure, albeit forming larger aggregates. On the other hand, *P. aeruginosa* grew into large, dense mat-like structures. The subsequent growth of mixed-species biomass was associated with distinct changes in spatial organization across the two species, with *S. aureus* aggregates embedded in the lower parts of, and surrounded by, the *P. aeruginosa* biomass. Further, the biomass composition of the mixed-species biomass revealed a predominance of *P. aeruginosa* over time, likely a result of interspecies interactions resulting in *P. aeruginosa* impairing the growth of *S. aureus* [21,99].

In chronic wound, *P. aeruginosa* and *S. aureus* biofilms show distinct spatial segregation, with *S. aureus* seen as smaller aggregates closer to the wound surface [6], and *P. aeruginosa* found as larger aggregates in the deeper regions of the wound. This has been partially attributed to the virulence features of *P. aeruginosa*, such as motility, destruction of polymorphonuclear leukocytes, adaptation to low-oxygen conditions and production of tissue remodeling enzymes [101–105]. It is important to note that this non-random distribution occurs over prolonged periods of time, and will therefore be influenced by immune factors and tissue remodeling. Given this, it is very likely that in the initial phases of bacterial colonization, *P. aeruginosa* and *S. aureus* co-exist in close proximity [23]. This could result from colonization with one pathogen predisposing establishment of the second pathogen, or infection with both pathogens could occur over short intervals of time. Regardless, the co-existence of both pathogens in the wound bed would result in a range of interactions, likely to influence the subsequent structure and organization of mixed-species biofilms. Based on our study, the structure and organization of early mixed-species biomass, notably the aggregate structure of *S. aureus*, appears to be influenced largely by the presence of the host cell substratum. On the other hand, subsequent biomass features and formation, are influenced by a combination of microenvironmental factors including the biochemical milieu and presence and growth of *P. aeruginosa* (Fig. 7). In clinical wounds, the prolonged effects of bacterial virulence factors, immune factors and tissue remodeling enzymes (not recapitulated in the 4-D microenvironment), such as *P. aeruginosa* elastases [103–105], could result in *P. aeruginosa* migrating to the deeper regions of the wound, while *S. aureus* remains as smaller aggregates closer to the wound surface.

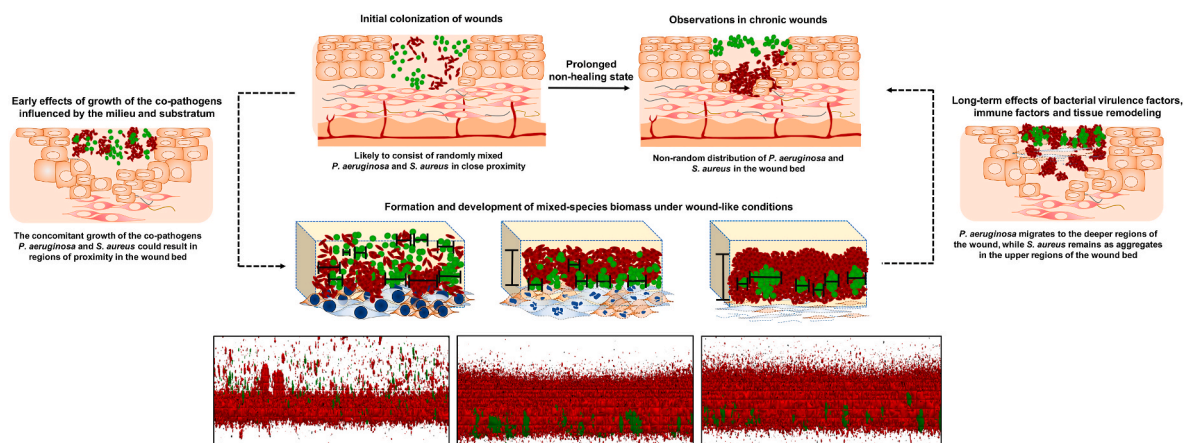


**Fig. 7. Proposed fine-tuned model of the structure and organization of mixed-species *P. aeruginosa* and *S. aureus* biofilms in the wound bed.** During initial colonization and growth in the wound bed, *P. aeruginosa* and *S. aureus* are likely to exist in regions of close proximity. In this study, the 4-D microenvironment recapitulates the concomitant and proximate presence of *P. aeruginosa* and *S. aureus* in the wound bed. The mixed-species biomass shows distinct structure and organization, seen as smaller aggregates of *S. aureus* embedded in large, dense, mat-like *P. aeruginosa* biofilms. Over time in clinical wounds, the combined effects of bacterial virulence factors, immune factors and tissue remodeling could result in *P. aeruginosa* migrating to the deeper regions of the wound, while *S. aureus* remains as small aggregates closer to the wound surface. This would result in the characteristic spatial distribution of *P. aeruginosa* and *S. aureus* seen in chronic, non-healing wounds. Representative images of mixed-species biomass in the 4-D wound microenvironment were rendered using Paraview v5.10.0.

#### 4. Conclusions and future directions

The 4-D microenvironment recapitulates key features of the wound infection state, such as a reconstructed host cell surface and wound milieu. We leveraged this recapitulated microenvironment to characterize the structure of mixed-species *P. aeruginosa* and *S. aureus* biofilms across multiple levels of organization. Overall, several features of the mixed-species biomass in the 4-D microenvironment align with clinical and *in vivo* observations of wound biofilms [7–9], such as the formation of biofilm aggregates, coexistence of both pathogens with a predominance of *P. aeruginosa*, and indication of possible inhibitory effects of *P. aeruginosa* on *S. aureus*. Further, the 4-D system also enabled a fine-tuned analysis of the influence of the host and pathogen relevant factors, such as the substratum, biochemical milieu, and interspecies interactions, on the structure and organization of the mixed-species biomass. Given this, the platform provides insights into mixed-species biomass features and formation when *P. aeruginosa* and *S. aureus* are in close proximity, which can be placed in the context of the current understanding of *P. aeruginosa* and *S. aureus* organization in the wound bed.

While the fixed co-cultured host cell scaffold provides a biomimetic substratum, the wound bed consists of proliferating and migrating keratinocytes and fibroblasts, which are likely to influence host-biofilm interactions. Given that maintaining host cell viability in the presence of bacterial growth poses technical challenges [106], fixed host cell scaffolds provide a semi-inert, 3-D biomimetic substratum for biofilm growth, and DAPI-stained nuclei indicate the presence of host cells in relation to the mixed-species biomass. While the presence of biofilms (in particular *P. aeruginosa*) is observed to destroy the host cell scaffold over time, from 8 h onwards, the *P. aeruginosa* biofilms observed are dense mats. Given this, the system, even at 48 h, lends itself well to study the various stages of biofilm formation (from initial attachment to biofilm aggregates to formation of dense, mature mats), and can possibly be extended or adapted to different biofilm growth stages with changes in media and bacterial inoculums. Nevertheless, the host cell component of the platform could be optimized to allow for the presence of live host cells that would more closely mimic the host cell-biofilm interface. This would be particularly relevant in the context of studying initial colonization and bacterial adherence in the wound bed. Further, when using live host cells, staining the two cell types (with cytoskeletal stains such as vimentin and cytokeratin [107,108]) would provide additional insights such as the location of the biofilm aggregates with respect to the host cell structure, as well as comparison across different host cell types. With the addition of live host cells, the 4-D platform can also be leveraged to monitor the inflammatory profile of keratinocytes and fibroblasts in the presence of biofilms, similar to this previous study with a 3D reconstructed human epidermis [68].

The 4-D microenvironment can also be expanded to study the viability of the mixed-species and single-species biomass grown in the system. For this, colony-forming units (CFUs) of the biomass could be used to measure changes in the biomass density and composition over time, as well as establish correlation between aggregate sizes and bacterial numbers (particularly in the context of *P. aeruginosa* outcompeting *S. aureus*). This is particularly interesting given the positive correlation between microscopy data and CFU counts from previous biofilm studies [109–111]. Along these lines, optimizing the platform for live-dead staining would provide further insights into the metabolic structure of the mixed-species biomass [54], which would be interesting given the chemical composition of the IVWM. Finally, visualization of the biofilm matrix or extracellular DNA components of the matrix could be used to characterize the roles of non-bacterial components in biofilm structure and organization [112].

Finally, to further the clinical relevance of the platform, the 4-D microenvironment can be used to study gene expression profiles of *P. aeruginosa* and *S. aureus* biofilms (as mixed-species and single-species), in comparison with standard laboratory media and

previously published reports in clinical wounds [113–115]. This would lend itself well to building the 4-D microenvironment into a platform for evaluating anti-biofilm approaches, such as antimicrobial agents and wound washes [68], with high-throughput structural and functional readouts. This would be particularly relevant in the context of clinical strains of *P. aeruginosa* and *S. aureus*, as well as other wound pathogens, and the next steps for this work would be to demonstrate and characterize biofilm formation with clinical strains in the 4-D microenvironment.

Overall, the 4-D wound microenvironment represents a composite *in vitro* model that can be leveraged to study the features and formation of *P. aeruginosa* and *S. aureus* mixed-species biofilms, and open hitherto unexplored insights into the structure and organization of biofilms under wound-relevant conditions. For this, the reconstructed nature of the platform lends itself well not only for multi-level and multi-parameter insights, but also for dissecting the roles of various host, matrix, biochemical, and microbial factors, as well as the interplays between them.

#### Funding

KSK's appointment is supported by the Ramalingaswami Re-entry Fellowship (BT/HRD/16/2006), Department of Biotechnology, Government of India. RD's appointment is supported by the Har Gobind Khorana-Innovative Young Biotechnologist Award (HGK-IYBA), Department of Biotechnology, Government of India to KSK (BT/12/IYBA/2019/05). This study is funded by the Har Gobind Khorana-Innovative Young Biotechnologist Award (HGK-IYBA), Department of Biotechnology, Government of India to KSK (BT/12/IYBA/2019/05).

#### Pre-print submission

This manuscript is submitted as a preprint to bioRxiv: <https://bioRxiv.org/cgi/content/short/2022.05.14.491929v1>.

#### CRediT authorship contribution statement

**Radhika Dhekane:** Methodology, Investigation, Validation, Writing – original draft. **Shreeya Mhade:** Methodology, Investigation, Validation, Writing – original draft. **Karishma S. Kaushik:** Conceptualization, Methodology, Formal analysis, Project administration, Supervision, Writing – original draft, Writing – review & editing, Funding acquisition.

#### Declaration of competing interest

The authors declare that they have no known competing financial interests or personal relationships that could have appeared to influence the work reported in this paper.

Given her role as Editor in 'Biofilm', Karishma S Kaushik was not involved in the peer review of this article and has no access to information regarding its peer review. Full responsibility for the editorial process for this article was delegated to Birthe Kjellerup.

#### Data availability

Data will be made available on request.

#### Acknowledgements

We thank M Vandana and Sujaya Ingale, NCL-Innovation Park, Pune, India for technical assistance with confocal microscopy.

#### Appendix A. Supplementary data

Supplementary data to this article can be found online at <https://doi.org/10.1016/j.biofilm.2022.100087>.

## References

- [1] James GA, Swogger E, Wolcott R, Pulcini ED, Secor P, Sestrich J, et al. Biofilms in chronic wounds. *Wound Repair Regen* 2008;16:37–44. <https://doi.org/10.1111/j.1524-475X.2007.00321.x>.
- [2] Malone M, Bjarnsholt T, McBain AJ, James GA, Stoodley P, Leaper D, et al. The prevalence of biofilms in chronic wounds: a systematic review and meta-analysis of published data. *J Wound Care* 2017;26:20–5. <https://doi.org/10.12968/jowc.2017.26.1.20>.
- [3] Clinton A, Carter T. Chronic wound biofilms: pathogenesis and potential therapies. *Lab Med* 2015;46:277–84. <https://doi.org/10.1309/LMBNSWKU14JPN7SO>.
- [4] Bjarnsholt T, Kirketerp-Møller K, Jensen PØ, Madsen KG, Phipps R, Kroghfelt K, et al. Why chronic wounds will not heal: a novel hypothesis. *Wound Repair Regen* 2008;16:2–10. <https://doi.org/10.1111/j.1524-475X.2007.00283.x>.
- [5] Fazli M, Bjarnsholt T, Kirketerp-Møller K, Jørgensen A, Andersen CB, Givskov M, et al. Quantitative analysis of the cellular inflammatory response against biofilm bacteria in chronic wounds. *Wound Repair Regen* 2011;19:387–91. <https://doi.org/10.1111/j.1524-475X.2011.00681.x>.
- [6] Fazli M, Bjarnsholt T, Kirketerp-Møller K, Jørgensen B, Andersen AS, Kroghfelt KA, et al. Nonrandom distribution of *Pseudomonas aeruginosa* and *Staphylococcus aureus* in chronic wounds. *J Clin Microbiol* 2009;47:4084–9. <https://doi.org/10.1128/JCM.01395-09>.
- [7] Kirketerp-Møller K, Jensen PØ, Fazli M, Madsen KG, Pedersen J, Moser C, et al. Distribution, organization, and ecology of bacteria in chronic wounds. *J Clin Microbiol* 2008;46:2717–22. <https://doi.org/10.1128/JCM.00501-08>.
- [8] Oates A, Bowling FL, Boulton AJM, Bowler PG, Metcalf DG, McBain AJ. The visualization of biofilms in chronic diabetic foot wounds using routine diagnostic microscopy methods. *2014 J Diabetes Res* 2014;15:3586. <https://doi.org/10.1155/2014/153586>.
- [9] Johani K, Malone M, Jensen S, Gosbell I, Dickson H, Hu H, et al. Microscopy visualisation confirms multi-species biofilms are ubiquitous in diabetic foot ulcers. *Int Wound J* 2017;14:1160–9. <https://doi.org/10.1111/iwj.12777>.
- [10] Malone M, Johani K, Jensen SO, Gosbell IB, Dickson HG, McLennan S, et al. Effect of cadexomer iodine on the microbial load and diversity of chronic non-healing diabetic foot ulcers complicated by biofilm in vivo. *J Antimicrob Chemother* 2017;72:2093–101. <https://doi.org/10.1093/jac/dkx099>.
- [11] Suryaletha K, John J, Radhakrishnan MP, George S, Thomas S. Metataxonomic approach to decipher the polymicrobial burden in diabetic foot ulcer and its biofilm mode of infection. *Int Wound J* 2018;15:473–81. <https://doi.org/10.1111/iwj.12888>.
- [12] Kirketerp-Møller K, Stewart PS, Bjarnsholt T. The zone model: a conceptual model for understanding the microenvironment of chronic wound infection. *Wound Repair Regen* 2020;28:593–9. <https://doi.org/10.1111/wrr.12841>.
- [13] Jordana-Lluich E, Garcia V, Kingdon ADH, Singh N, Alexander C, Williams P, et al. A simple polymicrobial biofilm keratinocyte colonization model for exploring interactions between commensals, pathogens and antimicrobials. *Front Microbiol* 2020;11:291. <https://doi.org/10.3389/fmicb.2020.00291>.
- [14] Chen YE, Fischbach MA, Belkaid Y. Skin microbiota-host interactions. *Nature* 2018;553:427–36. <https://doi.org/10.1038/nature25177>.
- [15] Çelebi-Saltik B, Kart D. Dermal fibroblast cells interactions with single and triple bacterial-species biofilms. *Mol Biol Rep* 2021;48:3393–404. <https://doi.org/10.1007/s11033-021-06391-0>.
- [16] Tuttle MS, Mostow E, Mukherjee P, Hu FZ, Melton-Kreft R, Ehrlich GD, et al. Characterization of bacterial communities in venous insufficiency wounds by use of conventional culture and molecular diagnostic methods. *J Clin Microbiol* 2011;49:3812–9. <https://doi.org/10.1128/JCM.00847-11>.
- [17] Orazi G, O'Toole GA. "It takes a village": mechanisms underlying antimicrobial recalcitrance of polymicrobial biofilms. *J Bacteriol* 2019;202. <https://doi.org/10.1128/JB.00530-19>.
- [18] DeLeon S, Clinton A, Fowler H, Everett J, Horswill AR, Rumbaugh KP. Synergistic interactions of *Pseudomonas aeruginosa* and *Staphylococcus aureus* in an in vitro wound model. *Infect Immun* 2014;82:4718–28. <https://doi.org/10.1128/IAI.02198-14>.
- [19] Serra R, Grande R, Butrico L, Rossi A, Settimio UF, Caroleo B, et al. Chronic wound infections: the role of *Pseudomonas aeruginosa* and *Staphylococcus aureus*. *Expert Rev Anti Infect Ther* 2015;13:605–13. <https://doi.org/10.1586/14787210.2015.1023291>.
- [20] Dalton T, Dowd SE, Wolcott RD, Sun Y, Watters C, Griswold JA, et al. An in vivo polymicrobial biofilm wound infection model to study interspecies interactions. *PLoS One* 2011;6:e27317. <https://doi.org/10.1371/journal.pone.0027317>.
- [21] Hotterbeekx A, Kumar-Singh S, Goossens H, Malhotra-Kumar S. In vivo and in vitro Interactions between *Pseudomonas aeruginosa* and *Staphylococcus* spp. *Front Cell Infect Microbiol* 2017;7:106. <https://doi.org/10.3389/fcimb.2017.00106>.
- [22] Pastar I, Nusbaum AG, Gil J, Patel SB, Chen J, Valdes J, et al. Interactions of methicillin resistant *Staphylococcus aureus* USA300 and *Pseudomonas aeruginosa* in polymicrobial wound infection. *PLoS One* 2013;8:e56846. <https://doi.org/10.1371/journal.pone.0056846>.
- [23] Alves PM, Al-Badi E, Withycombe C, Jones PM, Purdy KJ, Maddocks SE. Interaction between *Staphylococcus aureus* and *Pseudomonas aeruginosa* is beneficial for colonisation and pathogenicity in a mixed biofilm. *Pathog Dis* 2018;76:1–10. <https://doi.org/10.1093/femspd/fty003>.
- [24] Bahamondez-Canas TF, Heersema LA, Smyth HDC. Current status of in vitro models and assays for susceptibility testing for wound biofilm infections. *Biomedicine* 2019;7:34. <https://doi.org/10.3390/biomedicine7020034>.
- [25] Brackman G, Coenye T. In vitro and in vivo biofilm wound models and their application. In: Donelli G, editor. *Adv. Microbiol. Infect. Dis. Public heal*, vol. 897. Cham: Springer International Publishing; 2015. p. 15–32. <https://doi.org/10.1007/978-3-319-15002-2>.
- [26] Chen X, Thomsen TR, Winkler H, Xu Y. Influence of biofilm growth age, media, antibiotic concentration and exposure time on *Staphylococcus aureus* and *Pseudomonas aeruginosa* biofilm removal in vitro. *BMC Microbiol* 2020;20:264. <https://doi.org/10.1186/s12866-020-01947-9>.
- [27] Diepoltova A, Konecna K, Jandourek O, Nachtigal P. Study of the impact of cultivation conditions and peg surface modification on the in vitro biofilm formation of *Staphylococcus aureus* and *Staphylococcus epidermidis* in a system analogous to the Calgary biofilm device. *J Med Microbiol* 2021;70. <https://doi.org/10.1099/jmm.0.001371>.
- [28] Malic S, Hill KE, Playle R, Thomas DW, Williams DW. In vitro interaction of chronic wound bacteria in biofilms. *J Wound Care* 2011;20:569–70. <https://doi.org/10.12968/jowc.2011.20.12.569>.
- [29] Kragh KN, Hutchison JB, Melaugh G, Rodesney C, Roberts AEL, Irie Y, et al. Role of multicellular aggregates in biofilm formation. *mBio* 2016;7. <https://doi.org/10.1128/mBio.00237-16>.
- [30] Banin E, Vasil ML, Greenberg EP. Iron and *Pseudomonas aeruginosa* biofilm formation. *Proc Natl Acad Sci U S A* 2005;102:11076–81. <https://doi.org/10.1073/pnas.0504266102>.
- [31] Yang L, Hu Y, Liu Y, Zhang J, Ulstrup J, Molin S. Distinct roles of extracellular polymeric substances in *Pseudomonas aeruginosa* biofilm development. *Environ Microbiol* 2011;13:1705–17. <https://doi.org/10.1111/j.1462-2920.2011.02503.x>.
- [32] Shepherd J, Douglas I, Rimmer S, Swanson L, MacNeil S. Development of three-dimensional tissue-engineered models of bacterial infection of human skin wounds. *Tissue Eng C Methods* 2009;15:475–84. <https://doi.org/10.1089/ten.tec.2008.0614>.
- [33] Jensen LK, Johansen ASB, Jensen HE. Porcine models of biofilm infections with focus on pathomorphology. *Front Microbiol* 2017;8:1961. <https://doi.org/10.3389/fmicb.2017.01961>.
- [34] MacNeil S, Shepherd J, Smith L. Production of tissue-engineered skin and oral mucosa for clinical and experimental use. In: Haycock JW, editor. *3D cell culture protocol Methods in Molecular Biology*, vol. 695. Totowa, NJ: Humana Press; 2011. p. 129–53. [https://doi.org/10.1007/978-1-60761-984-0\\_9](https://doi.org/10.1007/978-1-60761-984-0_9).
- [35] Kadam S, Madhusoodhanan V, Dhekane R, Bhide D, Ugale R, Tikhole U, et al. Milieu matters: an in vitro wound milieu to recapitulate key features of, and probe new insights into, mixed-species bacterial biofilms. *Biofilms* 2021;3:100047. <https://doi.org/10.1016/j.biofilm.2021.100047>.
- [36] Kadam S, Nadkarni S, Lele J, Sakhalkar S, Mokashi P, Kaushik KS. Bioengineered platforms for chronic wound infection studies: how can we make them more human-relevant? *Front Bioeng Biotechnol* 2019;7:418. <https://doi.org/10.3389/fbioe.2019.00418>.
- [37] Kirker KR, James GA. In vitro studies evaluating the effects of biofilms on wound-healing cells: a review. *APMIS* 2017;125:344–52. <https://doi.org/10.1111/apm.12678>.
- [38] Thaarup IC, Bjarnsholt T. Current in vitro biofilm-infected chronic wound models for developing new treatment possibilities. *Adv Wound Care* 2021;10:91–102. <https://doi.org/10.1089/wound.2020.1176>.
- [39] Kucera J, Sojka M, Pavlik V, Szuszkiewicz K, Velebný V, Klein P. Multispecies biofilm in an artificial wound bed—A novel model for in vitro assessment of solid antimicrobial dressings. *J Microbiol Methods* 2014;103:18–24. <https://doi.org/10.1016/j.mimet.2014.05.008>.
- [40] Irie Y, Borlee BR, O'Connor JR, Hill PJ, Harwood CS, Wozniak DJ, et al. Self-produced exopolysaccharide is a signal that stimulates biofilm formation in *Pseudomonas aeruginosa*. *Proc Natl Acad Sci U S A* 2012;109. <https://doi.org/10.1073/pnas.1217993109>.
- [41] Malone CL, Boles BR, Lauderdale KJ, Thoendel M, Kavanaugh JS, Horswill AR. Fluorescent reporters for *Staphylococcus aureus*. *J Microbiol Methods* 2009;77:251–60. <https://doi.org/10.1016/j.mimet.2009.02.011>.
- [42] Wiegand I, Hilpert K, Hancock REW. Agar and broth dilution methods to determine the minimal inhibitory concentration (MIC) of antimicrobial substances. *Nat Protoc* 2008;3:163–75. <https://doi.org/10.1038/nprot.2007.521>.
- [43] Foxley MA, Friedline AW, Jensen JM, Nimmo SL, Scull EM, King JB, et al. Efficacy of ampicillin against methicillin-resistant *Staphylococcus aureus* restored through synergy with branched poly(ethyleneimine). *J Antibiot (Tokyo)* 2016;69:871–8. <https://doi.org/10.1038/ja.2016.44>.
- [44] Kadam S, Vandana M, Kaushik KS. Reduced serum methods for contact-based coculture of human dermal fibroblasts and epidermal keratinocytes. *Biotechniques* 2020;69:347–55. <https://doi.org/10.2144/btn-2020-0112>.
- [45] Hartmann R, Jeckel H, Jelli E, Singh PK, Vaidya S, Bayer M, et al. Quantitative image analysis of microbial communities with BiofilmQ. *Nat Microbiol* 2021;6:151–6. <https://doi.org/10.1038/s41564-020-00817-4>.
- [46] Drescher K. BiofilmQ v0.2.1. *BiofilmQ* 2020. <https://drescherlab.org/data/biofilmQ/>.
- [47] Otsu N. A threshold selection method from gray-level histograms. *IEEE Trans Syst Man Cybern* 1979;9:62–6. <https://doi.org/10.1109/TSMC.1979.4310076>.
- [48] Ahrens J, Geveci B, Law C. ParaView: an end-user tool for large-data visualization. In: Hansen Charles D, Johnson Chris R, editors. *Visualization Handbook*. Burlington: Butterworth-Heinemann; 2005. p. 717–31. <https://doi.org/10.1016/B978-012387582-2/50038-1>.
- [49] Ayachit U. The ParaView guide: a parallel visualization application. Clifton Park, NY, USA: Kitware, Inc.; 2015. <https://doi.org/10.5555/2789330>.
- [50] ParaView. ParaView v5.10.0. *ParaView*, <https://www.paraview.org/>; 2021.

- [51] Abramoff M, Magalhães P, Ram SJ. Image processing with ImageJ. *Biophot Int* 2004;11:36–42.
- [52] Schneider CA, Rasband WS, Eliceiri KW. NIH Image to ImageJ: 25 years of image analysis. *Nat Methods* 2012;9:671–5. <https://doi.org/10.1038/nmeth.2089>.
- [53] Blanchette-Cain K, Hinojosa CA, Akula Suresh Babu R, Lizcano A, Gonzalez-Juarbe N, Munoz-Almagro C, et al. *Streptococcus pneumoniae* biofilm formation is strain dependent, multifactorial, and associated with reduced invasiveness and immunoreactivity during colonization. *mBio* 2013;4. <https://doi.org/10.1128/mBio.00745-13>. 007455-13.
- [54] Singh N, Romero M, Travanut A, Monteiro PF, Jordana-Lluch E, Hardie KR, et al. Dual bioresponsive antibiotic and quorum sensing inhibitor combination nanoparticles for treatment of *Pseudomonas aeruginosa* biofilms in vitro and ex vivo. *Biomater Sci* 2019;7:4099–111. <https://doi.org/10.1039/c9bm00773c>.
- [55] GraphPad. GraphPad Prism version 6.01 for Windows. San Diego, Calif USA: GraphPad Software; 2022. [www.graphpad.com](http://www.graphpad.com).
- [56] Li Y, Kilian KA. Bridging the gap: from 2D cell culture to 3D microengineered extracellular matrices. *Adv Healthc Mater* 2015;4:2780–96. <https://doi.org/10.1002/adhm.201500427>.
- [57] Sun M, Liu A, Yang X, Gong J, Yu M, Yao X, et al. 3D cell culture—can it be as popular as 2D cell culture? *Adv NanoBiomed Res* 2021;1:2000066. <https://doi.org/10.1002/anbr.202000066>.
- [58] Peabworth M-P, Cismas SA, Asuri P. A novel 2.5D culture platform to investigate the role of stiffness gradients on adhesion-independent cell migration. *PLoS One* 2014;9:e110453. <https://doi.org/10.1371/journal.pone.0110453>.
- [59] Langhans SA. Three-dimensional in vitro cell culture models in drug discovery and drug repositioning. *Front Pharmacol* 2018;9:6. <https://doi.org/10.3389/fphar.2018.00006>.
- [60] Powell K. Adding depth to cell culture. 80- *Science* 2017;96–8. <https://doi.org/10.1126/science.opms.p1700113>.
- [61] Hilderbrand AM, Ovadia EM, Rehmann MS, Kharkar PM, Guo C, Kloxin AM. Biomaterials for 4D stem cell culture. *Curr Opin Solid State Mater Sci* 2016;20:212–24. <https://doi.org/10.1016/j.cossms.2016.03.002>.
- [62] Miao S, Cui H, Esworthy T, Mahadik B, Lee S, Zhou X, et al. 4D self-morphing culture substrate for modulating cell differentiation. *Adv Sci* 2020;7:1902403. <https://doi.org/10.1002/advs.201902403>.
- [63] Zheng Y, Liang Han MK, Jiang Q, Li B, Feng J, del Campo A. 4D hydrogel for dynamic cell culture with orthogonal, wavelength-dependent mechanical and biochemical cues. *Mater Horiz* 2020;7:111–6. <https://doi.org/10.1039/C9MH00665F>.
- [64] Zhao J, Wang R, Zhang J, Zhao Y, Qiao S, Crouzier T, et al. A novel 4D cell culture mimicking stomach peristalsis altered gastric cancer spheroids growth and malignance. *Biofabrication* 2021;13:035034. <https://doi.org/10.1088/1758-5090/abf6bf>.
- [65] Percival SL, McCarty SM, Lipsky B. Biofilms and wounds: an overview of the evidence. *Adv Wound Care* 2015;4:373–81. <https://doi.org/10.1089/wound.2014.0557>.
- [66] Trengove NJ, Stacey MC, Macauley S, Bennett N, Gibson J, Burslem F, et al. Analysis of the acute and chronic wound environments: the role of proteases and their inhibitors. *Wound Repair Regen* 1999;7:442–52. <https://doi.org/10.1046/j.1524-475X.1999.00442.x>.
- [67] Trengove NJ, Langton SR, Stacey MC. Biochemical analysis of wound fluid from nonhealing and healing chronic leg ulcers. *Wound Repair Regen* 1996;4:234–9. <https://doi.org/10.1046/j.1524-475X.1996.40211.x>.
- [68] Brown JL, Townsend E, Short RD, Williams C, Woodall C, Nile CJ, et al. Assessing the inflammatory response to in vitro polymicrobial wound biofilms in a skin epidermis model. *Npj Biofilms Microbiomes* 2022;8:19. <https://doi.org/10.1038/s41522-022-00286-z>.
- [69] Jones JD, Ramser HE, Woessner AE, Quinn KP. In vivo multiphoton microscopy detects longitudinal metabolic changes associated with delayed skin wound healing. *Commun Biol* 2018;1:198. <https://doi.org/10.1038/s42003-018-0206-4>.
- [70] Schaudinn C, Dittmann C, Jurisch J, Laue M, Günday-Türelı N, Blume-Peytavi U, et al. Development, standardization and testing of a bacterial wound infection model based on ex vivo human skin. *PLoS One* 2017;12:e0186946. <https://doi.org/10.1371/journal.pone.0186946>.
- [71] Hurlow J, Blanz E, Gaddy JA. Clinical investigation of biofilm in non-healing wounds by high resolution microscopy techniques. *J Wound Care* 2016;25: S11–22. <https://doi.org/10.12968/jowc.2016.25.Sup9.S11>.
- [72] Yoon DJ, Fregoso DR, Nguyen D, Chen V, Strbo N, Fuentes JJ, et al. A tractable, simplified ex vivo human skin model of wound infection. *Wound Repair Regen* 2019;27:421–5. <https://doi.org/10.1111/wrr.12712>.
- [73] Wojtowicz AM, Oliveira S, Carlson MW, Zawadzka A, Rousseau CF, Baksh D. The importance of both fibroblasts and keratinocytes in a bilayered living cellular construct used in wound healing. *Wound Repair Regen* 2014;22:246–55. <https://doi.org/10.1111/wrr.12154>.
- [74] Menon SN, Flegg JA, McCue SW, Schugart RC, Dawson RA, McElwain DLS. Modelling the interaction of keratinocytes and fibroblasts during normal and abnormal wound healing processes. *Proc R Soc B Biol Sci* 2012;279:3329–38. <https://doi.org/10.1098/rspb.2012.0319>.
- [75] Bullock AJ, Garcia M, Shepherd J, Rehman I, Sheila M. Bacteria induced pH changes in tissue-engineered human skin detected non-invasively using Raman confocal spectroscopy. *Appl Spectrosc Rev* 2020;55:158–71. <https://doi.org/10.1080/05704928.2018.1558232>.
- [76] Hashimoto K, Yamashita K, Enoyoshi K, Dahan X, Takeuchi T, Kori H, et al. The effects of coating culture dishes with collagen on fibroblast cell shape and swirling pattern formation. *J Biol Phys* 2020;46:351–69. <https://doi.org/10.1007/s10867-020-09556-3>.
- [77] Gabbott CM, Sun T. Comparison of human dermal fibroblasts and HaCat cells cultured in medium with or without serum via a generic tissue engineering research platform. *Int J Mol Sci* 2018;19:388. <https://doi.org/10.3390/ijms19020388>.
- [78] Wong C-W, LeGrand CF, Kinnear BF, Sobota RM, Ramalingam R, Dye DE, et al. In vitro expansion of keratinocytes on human dermal fibroblast-derived matrix retains their stem-like characteristics. *Sci Rep* 2019;9:18561. <https://doi.org/10.1038/s41598-019-54793-9>.
- [79] Qin Z, He T, Guo C, Quan T. Age-related downregulation of CCN2 is regulated by cell size in a YAP/TAZ-Dependent manner in human dermal fibroblasts: impact on dermal aging. *JID Innov Ski Sci from Mol to Popul Heal* 2022;2:100111. <https://doi.org/10.1016/j.xjidi.2022.100111>.
- [80] Freitas Jr R. Vol. I Basic Capab. In: *Cytometrics. Nanomedicine, vol. 1. Texas, US: Georgetown; 1999. p. 247. Landes Bioscience.*
- [81] Watt FM, Green H. Involucrin synthesis is correlated with cell size in human epidermal cultures. *J Cell Biol* 1981;90:738–42. <https://doi.org/10.1083/jcb.90.3.738>.
- [82] Bourkoulas A, Constantoudis V, Kontziampis D, Petrou PS, Kakabakos SE, Tseripi A, et al. Roughness threshold for cell attachment and proliferation on plasma micro-nanotextured polymeric surfaces: the case of primary human skin fibroblasts and mouse immortalized 3T3 fibroblasts. *J Phys D Appl Phys* 2016;49: 1–10. <https://doi.org/10.1088/0022-3727/49/30/304002>.
- [83] Moore MJ, Sebastian JA, Kolios MC. Determination of cell nucleus-to-cytoplasmic ratio using imaging flow cytometry and a combined ultrasound and photoacoustic technique: a comparison study. *J Biomed Opt* 2019;24:1–10. <https://doi.org/10.1117/1.JBO.24.10.106502>.
- [84] Kumar P, Kedaria D, Mahapatra C, Mohandas M, Chatterjee K. A designer cell culture insert with a nanofibrous membrane toward engineering an epithelial tissue model validated by cellular nanomechanics. *Nanoscale Adv* 2021;3: 4714–25. <https://doi.org/10.1039/D1NA00280E>.
- [85] Bao M, Xie J, Piruska A, Huck WTS. 3D microniches reveal the importance of cell size and shape. *Nat Commun* 2017;8:1962. <https://doi.org/10.1038/s41467-017-02163-2>.
- [86] Chu F-Y, Haley SC, Zidovska A. On the origin of shape fluctuations of the cell nucleus. *Proc Natl Acad Sci U S A* 2017;114:10338–43. <https://doi.org/10.1073/pnas.1702226114>.
- [87] Vukovic LD, Jevtic P, Edens LJ, Levy DL. New insights into mechanisms and functions of nuclear size regulation. In: Jeon KW, editor. *International Review of Cell and Molecular Biology, vol. 322. Academic Press; 2016. p. 1–59. https://doi.org/10.1016/bs.ircmb.2015.11.001.*
- [88] Watters C, DeLeon K, Trivedi U, Griswold JA, Lyte M, Hampel KJ, et al. *Pseudomonas aeruginosa* biofilms perturb wound resolution and antibiotic tolerance in diabetic mice. *Med Microbiol Immunol* 2013;202:131–41. <https://doi.org/10.1007/s00430-012-0277-7>.
- [89] Sønderholm M, Kragh KN, Koren K, Jakobsen TH, Darch SE, Alhede M, et al. *Pseudomonas aeruginosa* aggregate formation in an alginate bead model system exhibits in vivo-like characteristics. *Appl Environ Microbiol* 2017;83:1–15. <https://doi.org/10.1128/AEM.00113-17>.
- [90] Alhede M, Lorenz M, Fritz BG, Jensen PØ, Ring HC, Bay L, et al. Bacterial aggregate size determines phagocytosis efficiency of polymorphonuclear leukocytes. *Med Microbiol Immunol* 2020;209:669–80. <https://doi.org/10.1007/s00430-020-00691-1>.
- [91] Bay L, Kragh KN, Eickhardt SR, Poulsen SS, Gjerdrum LMR, Ghatiani K, et al. Bacterial aggregates establish at the edges of acute epidermal wounds. *Adv Wound Care* 2018;7:105–13. <https://doi.org/10.1089/wound.2017.0770>.
- [92] Haaber J, Cohn MT, Frees D, Andersen TJ, Ingmer H. Planktonic aggregates of *Staphylococcus aureus* protect against common antibiotics. *PLoS One* 2012;7: e41075. <https://doi.org/10.1371/journal.pone.0041075>.
- [93] Schleheck D, Barraud N, Klebensberger J, Webb JS, McDougald D, Rice SA, et al. *Pseudomonas aeruginosa* PAO1 preferentially grows as aggregates in liquid batch cultures and disperses upon starvation. *PLoS One* 2009;4:e5513. <https://doi.org/10.1371/journal.pone.0005513>.
- [94] Alhede M, Kragh KN, Qvortrup K, Allesen-Holm M, van Gennip M, Christensen LD, et al. Phenotypes of non-attached *Pseudomonas aeruginosa* aggregates resemble surface attached biofilm. *PLoS One* 2011;6:e27943. <https://doi.org/10.1371/journal.pone.0027943>.
- [95] Knott S, Curry D, Zhao N, Metgud P, Dastgheyb SS, Purtil C, et al. *Staphylococcus aureus* floating biofilm formation and phenotype in synovial fluid depends on albumin, fibrinogen, and hyaluronic acid. *Front Microbiol* 2021;12:1–13. <https://doi.org/10.3389/fmicb.2021.655873>.
- [96] Crosby HA, Kwiecinski J, Horswill AR. *Staphylococcus aureus* aggregation and coagulation mechanisms, and their function in host-pathogen interactions. *Adv Appl Microbiol* 2016;96:1–41. <https://doi.org/10.1016/bs.aams.2016.07.018>.
- [97] Cai Y-M. Non-surface attached bacterial aggregates: a ubiquitous third lifestyle. *Front Microbiol* 2020;11:557035. <https://doi.org/10.3389/fmicb.2020.557035>.
- [98] Melaugh G, Hutchison J, Kragh KN, Irie Y, Roberts A, Bjarnsholt T, et al. Shaping the growth behaviour of biofilms initiated from bacterial aggregates. *PLoS One* 2015;11:e0149683. <https://doi.org/10.1371/journal.pone.0149683>.
- [99] Price CE, Brown DG, Limoli DH, Phelan VV, O'Toole GA. Exogenous alginate protects *Staphylococcus aureus* from killing by *Pseudomonas aeruginosa*. *J Bacteriol* 2020;202:1–17. <https://doi.org/10.1128/JB.00559-19>.
- [100] Chen X, Lorenzen J, Xu Y, Jonikaite M, Thaarup IC, Bjarnsholt T, et al. A novel chronic wound biofilm model sustaining coexistence of *Pseudomonas aeruginosa* and *Staphylococcus aureus* suitable for testing of antibiofilm effect of antimicrobial solutions and wound dressings. *Wound Repair Regen* 2021;29: 820–9. <https://doi.org/10.1111/wrr.12944>.

- [101] Klausen M, Heydorn A, Ragas P, Lamberts L, Aaes-Jørgensen A, Molin S, et al. Biofilm formation by *Pseudomonas aeruginosa* wild type, flagella and type IV pili mutants. *Mol Microbiol* 2003;48:1511–24. <https://doi.org/10.1046/j.1365-2958.2003.03525.x>.
- [102] Borer B, Tecon R, Or D. Spatial organization of bacterial populations in response to oxygen and carbon counter-gradients in pore networks. *Nat Commun* 2018;9:769. <https://doi.org/10.1038/s41467-018-03187-y>.
- [103] Kamath S, Kapatral V, Chakrabarty AM. Cellular function of elastase in *Pseudomonas aeruginosa*: role in the cleavage of nucleoside diphosphate kinase and in alginate synthesis. *Mol Microbiol* 1998;30:933–41. <https://doi.org/10.1046/j.1365-2958.1998.01121.x>.
- [104] Wretling B, Pavlovskis OR. *Pseudomonas aeruginosa* elastase and its role in pseudomonas infections. *Rev Infect Dis* 1983;5(Suppl 5):S998–1004. [https://doi.org/10.1093/clinids/5.supplement\\_5.s998](https://doi.org/10.1093/clinids/5.supplement_5.s998).
- [105] Prasad ASB, Shruptha P, Prabhu V, Srujan C, Nayak UY, Anuradha CKR, et al. *Pseudomonas aeruginosa* virulence proteins pseudolysin and protease IV impede cutaneous wound healing. *Lab Invest* 2020;100:1532–50. <https://doi.org/10.1038/s41374-020-00478-1>.
- [106] Crabbe A, Liu Y, Matthijs N, Rigole P, De La Fuente-Nunez C, Davis R, et al. Antimicrobial efficacy against *Pseudomonas aeruginosa* biofilm formation in a three-dimensional lung epithelial model and the influence of fetal bovine serum. *Sci Rep* 2017;7. <https://doi.org/10.1038/srep43321>.
- [107] Taghiabadi E, Mohammadi P, Aghdami N, Falah N, Orouji Z, Nazari A, et al. Treatment of hypertrophic scar in human with autologous transplantation of cultured keratinocytes and fibroblasts along with fibrin glue. *Cell J* 2015;17:49–58. <https://doi.org/10.22074/cellj.2015.511>.
- [108] Kuburich NA, den Hollander P, Pietz JT, Mani SA. Vimentin and cytokeratin: good alone, bad together. *Semin Cancer Biol* 2021. <https://doi.org/10.1016/j.semcancer.2021.12.006>.
- [109] Awasthi AK, Gupta S, Thakur J, Gupta S, Pal S, Bajaj A, et al. Polydopamine-on-liposomes: stable nanoformulations, uniform coatings and superior antifouling performance. *Nanoscale* 2020;12:5021–30. <https://doi.org/10.1039/c9nr07770g>.
- [110] Carvalho FG de, Puppim-Rontani RM, Fúcio SBP de, Negrini T de C, Carlo HL, Garcia-Godoy F. Analysis by confocal laser scanning microscopy of the MDPB bactericidal effect on *S. mutans* biofilm CLSM analysis of MDPB bactericidal effect on biofilm. *J Appl Oral Sci* 2012;20:568–75. <https://doi.org/10.1590/s1678-77572012000500013>.
- [111] Harrison JJ, Ceri H, Yerly J, Stremick CA, Hu Y, Martinuzzi R, et al. The use of microscopy and three-dimensional visualization to evaluate the structure of microbial biofilms cultivated in the calgary biofilm device. *Biol Proced Online* 2006;8:194–215. <https://doi.org/10.1251/bpo127>.
- [112] Karygianni L, Ren Z, Koo H, Thurnheer T. Biofilm matrixome: extracellular components in structured microbial communities. *Trends Microbiol* 2020;28:668–81. <https://doi.org/10.1016/j.tim.2020.03.016>.
- [113] D'Arpa P, Karna SLR, Chen T, Leung KP. *Pseudomonas aeruginosa* transcriptome adaptations from colonization to biofilm infection of skin wounds. *Sci Rep* 2021;11:20632. <https://doi.org/10.1038/s41598-021-00073-4>.
- [114] Karna SLR, D'Arpa P, Chen T, Qian L-W, Fourcaudot AB, Yamane K, et al. RNA-seq transcriptomic responses of full-thickness dermal excision wounds to *Pseudomonas aeruginosa* acute and biofilm infection. *PLoS One* 2016;11:e0165312. <https://doi.org/10.1371/journal.pone.0165312>.
- [115] Karash S, Nordell R, Ozer EA, Yahr TL. Genome sequences of two *Pseudomonas aeruginosa* isolates with defects in type III secretion system gene expression from a chronic ankle wound infection. *Microbiol Spectr* 2021;9:e0034021. <https://doi.org/10.1128/Spectrum.00340-21>.